Coastal Urban Atmospheric Mercury Cycling and Emissions in Boston, MA

by

Emma Rutkowski

Submitted to the Department of Earth, Atmospheric and Planetary
Sciences in partial fulfillment of the requirements for the degree of

Bachelor of Science in Earth, Atmospheric and Planetary Sciences
at the
MASSACHUSETTS INSTITUTE OF TECHNOLOGY

May 2019

Signature redacted

Author... ....
Department of Earth, Atmospheric and Planetary Science
May 17, 2019

Signature redacted

Certified by..
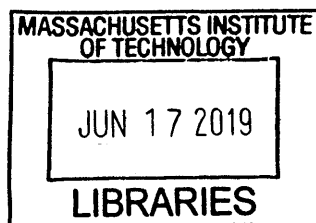Noelle Selin
Thesis Supervisor

Signature redacted

Accepted By..
Richard P. Binzel
Chair, Committee on Undergraduate Program

Abstract

This study aims to contribute to the body of knowledge regarding mercury emissions by reporting on a coastal, urban setting subject to inputs from both anthropogenic and oceanic reservoirs, in order to improve related policy decisions. Mercury can have serious health and ecological consequences, but the chemistry, transport and deposition of gaseous elemental mercury (Hg^0) are still not well understood. Estimates of anthropogenic emissions also remain uncertain. To better constrain urban- and regional-scale chemistry and emissions in a specifically coastal environment, concentrations of Hg^0 were measured at an urban site in Boston, MA from Aug 2017 to Sept 2018. The recorded concentrations were compared against supplementary records of several additional pollutants and meteorological variables. Concentrations in Boston were found to be relatively low, but follow diurnal and seasonal trends previously observed in other sites in the United States driven by meteorology. Further, back-trajectory and potential source contribution function analysis revealed oceanic re-emission of legacy deposits is a major input of Hg^0 to the Boston area, but no influence from specific large anthropogenic point sources was discernible in the data. A one box model was developed to represent the physical processes controlling Hg^0 concentrations in Boston in order to replicate concentrations, capture the difference in concentrations from land and ocean sources, and estimate both anthropogenic and oceanic emissions. Results from the box model analysis show the sensitivity of local Hg^0 concentrations to varying assumptions of mixing, background flux, meteorology, and emissions, and indicate that oceanic emissions and anthropogenic emissions are likely both higher than current estimates. The results of this study indicate the ocean plays a major role in Hg^0 cycling in coastal areas and provides motivation for further improvement of models to better capture local sources and cycling.

Acknowledgement

Contents

Introduction 1

Mercury is a heavy metal which exists in multiple forms in various Earth systems and can be detrimental to human and ecological health. In the atmosphere, mercury is present as elemental Hg^0, or as short-lived gaseous or particulate oxidized Hg(II), and the total reservoir is estimated to be between 4400 and 5300 Mg, enriched by 3 to 5 times from pre-industrial levels (Amos et al 2013; Outridge et al. 2018). However, there are still many uncertainties in estimates of both direct anthropogenic emissions and revolatilization of legacy deposits from soil and water bodies, which together account for 87% of all inputs to the atmosphere (Obrist et al 2018). In addition, the mechanisms by which mercury cycles between the atmosphere, ocean and terrestrial reservoirs are poorly understood. This study seeks to contribute to and improve on the existing body of knowledge by providing an ongoing record and analysis of gaseous elemental mercury at a site in Boston, Massachusetts.

1.1 Motivation

1.1.1 Adverse Health Effects

Mercury is a highly toxic heavy metal which can have detrimental effects on the health of humans exposed to it, and so effective regulation is crucial for protecting human health. One of the major routes of exposure for humans to mercury is via ingestion of methylmercury, which forms in aquatic ecosystems from the biological methylation of deposited Hg(II) (Jensen and Jernerlov 1969). Elemental gaseous mercury in the atmosphere can deposit directly to water bodies where it is oxidized to Hg(II) and then converted to MeHg, or can be oxidized in the atmosphere and then be deposited into

waterways, where it undergoes methylation (Obrist 2018, Soerensen et al. 2016). MeHg accumulates in fish higher up the food chain, and when consumed by humans is a neurotoxin, causing fatal poisoning in extreme cases (Harada 1995). Epidemiological studies in the Faroe Islands, Seychelles, and New Zealand suggest prenatal mercury exposure lowers childhood IQ even in non-extreme cases (Grandjean et al. 1997; Crump et al. 1998; Davidson et al. 1996; Myers et al. 2003) with a dose-response relationship of -0.18 IQ points for each part per million increase in mercury in maternal hair (Axelrad et al. 2007). Mercury exposure is also statistically associated with cardiovascular disease (Clarkson et al 2003).

Around small scale gold mines, inhalation and ingestion of inorganic mercury are major exposure pathways (Obiri et al. 2016; Gibb and O'Leary 2014). Dental amalgams or liquid mercury spills can also be sources for inhaled gaseous mercury, but the toxicology of these pathways is far more uncertain (Clarkson et al 2003). Certain groups are at increased risk due to socioeconomic, genetic, or biological factors. The effects of MeHg as a neurotoxin are particularly acute for pregnant women and children, and groups which rely on high-fish diets, especially coastal indigenous peoples and low-income anglers who often target predatory fish with enhanced MeHg concentrations, have high risk of exposure. Small scale gold mining disproportionately exposes workers in low income communities to high concentrations of Hg^0 (Eagles-Smith et al. 2018).

1.1.2 Current Regulations

Despite its high toxicity, several key guidelines for mercury emissions have gone into effect only recently, since 2015 (US EPA 2019). Understanding mercury cycling and emissions is crucial for monitoring the efficacy of new regulations and continuing to strengthen pollution controls.

The US ratified the Minamata Convention on Mercury in 2013, an international treaty which entered into force in 2017. The Minamata Convention seeks to control anthropogenic mercury emissions by banning new mercury mines, phasing mercury out of some products and processes, and regulating small-scale gold mining, and addresses storage, contaminated sites, disposal and health risks (Selin et al. 2018). As of May 2019, 128 nations have signed on and 107 have ratified the convention (Minamata Convention on Mercury 2019).

The United States Environmental Protection Agency (EPA) sets limits on emissions of Hg from coal and oil-fired power plants via the Mercury and Air Toxics Standards (MATS) under the authority of 1990 amendments to the Clean Air Act. The emissions limitations are technology-based and dictate that all plants must achieve emission reductions as high as the average achieved by the top 12% best performing facilities. These standards are

based on section 112 of the Clean Air Act, which calls for maximum achievable emission reductions, based on available technology, for all major point sources falling under the authority of the section. The EPA first released a study determining regulating mercury emissions from power plants was appropriate in 2000, but the final rules were not issued until December 2011. Under the rule, existing plants were all given 3 years to comply with the MATS, and permitting authorities were able to grant up to an extra year for "technology installation", bringing all plants into compliance by the end of 2015 (US EPA 2018).

In 2015, the Supreme Court decision in *Michigan v. EPA* found the EPA erred in not considering compliance costs when regulating emissions from coal and oil-fired electric utility steam generating units (EGUs). In response, the EPA prepared and solicited public comment on a supplemental finding which upheld that when considering costs, regulations were still appropriate and that EGU's should be included under the guidelines of section 112 (80 Fed. Reg. 75025. 2015; US EPA 2019).

In December of 2018 the EPA changed position, proposing a revised cost finding on the benefits of the MATS for EGUs. As of February 2019 the US EPA began accepting comments on proposed changes to the MATS. The EPA proposes to find that based on the cost of compliance, regulation of hazardous air pollutants such as mercury from EGU's is not "appropriate and necessary". Further, it proposes to find that risks due to emissions from the EGU point source category are acceptable based on risk analysis and no further emission controls or updates to MATS are necessary, and to collect comments on whether the EPA has the authority to rescind emission standards for EGU's (US EPA 2019). At the time of writing, the MATS remain in effect although the future of the regulations is uncertain.

1.2 Background

1.2.1 The Mercury Cycle

Mercury occurs naturally in the Earth's crust and is released via tectonic activity (Gustin et al 2000), with the main sink being deep-sediment burial. Mercury may cycle between the atmosphere, terrestrial systems and ocean for centuries to millennia before being removed (Selin 2009). Aside from geogenic emissions, mercury enters the atmosphere via biomass burning, legacy re-emissions from soil and water, and anthropogenic activity. The main routes of removal from the atmosphere are dry and wet deposition (Obrist 2018). Mercury in the atmosphere may exist in two forms, Hg^0 and $Hg(II)$, and cycles between these forms via oxidation and reduction reactions. Recent research suggests vegetation uptake provides a major route of removal of Hg^0, and controls seasonal variations in atmospheric mercury concentrations, which have been observed to peak in

winter and be at a low in summer (Jiskra et al 2018). Figure 1.1 summarizes the main physical processes and emission sources governing mercury cycling. The lifetime of Hg^0 in the atmosphere is approximately 0.5-1 year, which allows it to circulate and deposit far from the source (Selin et al 2007; Horowitz et al., 2017).
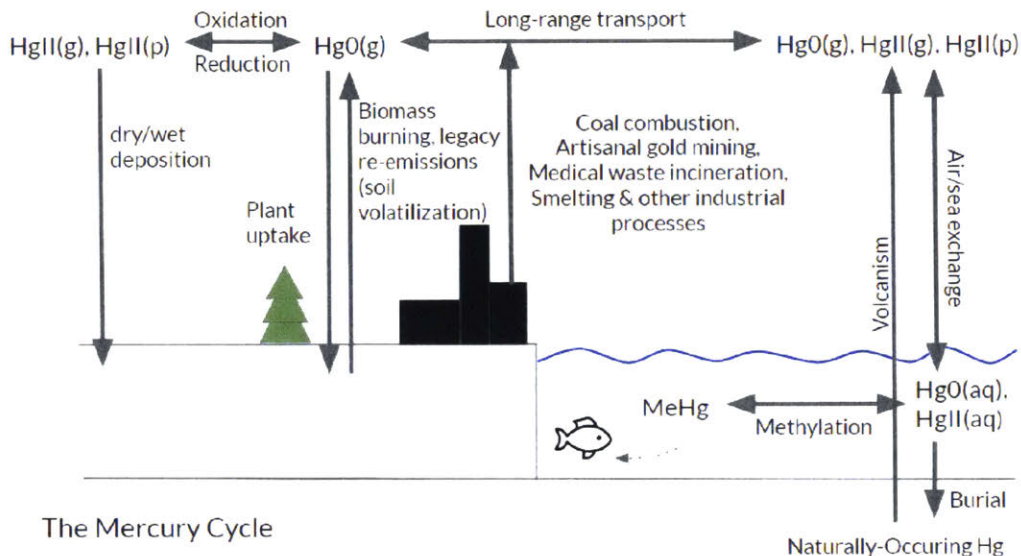

Fig. 1.1: An overview of the mercury cycle and sources for gaseous elemental mercury ($Hg^0(g)$), gaseous oxidized mercury ($Hg^{II}(g)$), particulate-bound oxidized mercury ($Hg^{II}(p)$), and methylmercury (MeHg). Mercury is released to the atmosphere via anthropogenic and geogenic sources. Other inputs to the atmosphere are re-volatilization of previously deposited mercury in soils and water bodies. Mercury is removed from the atmosphere via dry and wet deposition, and plant uptake.

Anthropogenic emissions of mercury increased significantly during the industrial revolution, with atmospheric concentrations peaking around 1970 (Fain et al 2009), and primary anthropogenic emissions make up approximately 27% of all atmospheric inputs (Amos et al. 2013). The major sources of anthropogenic emissions are artisanal gold mining and coal burning, with some other small contributions from medical and other waste incineration and smelting (UNEP 2018). However, there is little global data available that directly measures the contributions of gold mining and waste incineration, as well as other potential sources such as cement, steel and iron production (Obrist 2018). Another 60% of mercury input to the atmosphere is the result of volatilization of previously-deposited mercury in soils and water systems, which originally had an anthropogenic source (Amos et al 2013). Emissions globally increased by about 20% between 2010 and 2015, with small decreases in emissions in North America and Europe offset by increased industrial activity in the rest of the world (UNEP 2018).

1.2.2 Emissions Inventories

Two major federal programs collect mercury air emission inventories in the United States. Under the Emergency Planning and Community Right-to-Know Act, all industrial and federal facilities must report yearly emissions of mercury (among other toxic chemicals), as part of the Toxics Release Inventory (TRI) program. TRI provides a yearly record of mercury emissions for all facilities which meet the criteria to compel reporting. Any facility which employs ten or more people, manufactures, process or uses a TRI-listed chemical in quantities above the yearly threshhold, and falls under a specific industry sector must submit yearly TRI reports. The sectors covered by TRI are mining, utilities, manufacturing, merchant wholesalers, wholesale electronics, publishing, hazardous waste and federal facilities. TRI mandates reporting of fugitive air emissions and stack air emissions, in addition to numerous other forms of releases into land and water (US EPA 2019).
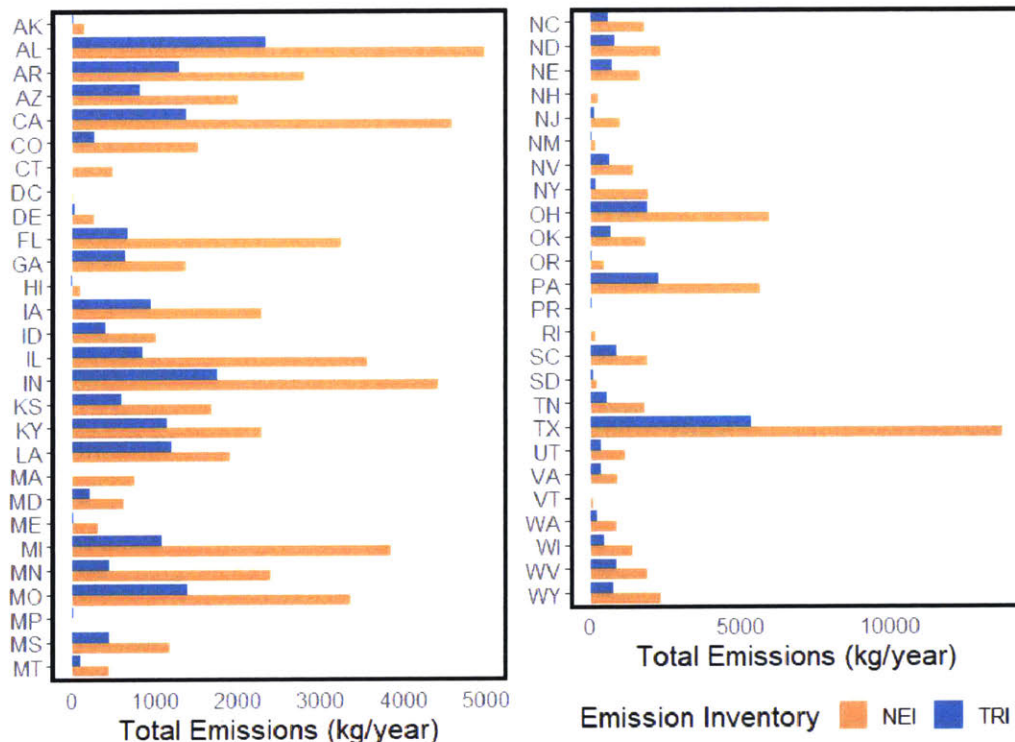

Fig. 1.2: The total state-by-state releases recorded in the NEI and TRI emission inventories for 2014. Bar labels denote the abbreviation of the state for which emissions are given, ie. AK = Alaska, AL = Alabama, etc. Typically NEI reports higher emissions due to the inclusion of onroad/offroad and non-point sources.

The National Emissions Inventory (NEI) provides a more comprehensive estimate of air emissions of mercury and other pollutants in the United States, although it has a coarser time resolution. NEI estimates are collected every 3 years, with the most recently

available inventory dating from 2014. NEI includes 5 main categories of emissions, listed in Table 1.1:

Category	Included Sources
Point Sources	Large/small industrial facilities, power plants, commercial facilities, portable asphalt operations
Nonpoint Sources	Sources too small individually to count as point sources, included as county total - residential heating, commercial combustion, asphalt paving, and commercial and consumer solvent use
Onroad Sources	Gasoline and diesel powered heavy and light duty vehicles operated on roads, highway ramps, and idling
Nonroad Sources	Gasoline and diesel powered mobile sources operated off-road - construction, aircraft ground support, lawn and garden equipment, locomotives, and commercial marine vessels
Event Sources	Wildfires and prescribed burns

Table 1.1: Emission categories included in NEI (US EPA 2019)

Figure 1.2 shows the total state-by-state releases recorded in the NEI and TRI emission inventories in 2014. Total Hg^0 emissions are 65% lower in TRI than NEI. Berg (2016) found that the absence of mining in TRI led to major discrepancies in the emission totals between the two inventories, with better agreement in the utilities sector. Additionally, large year-to-year variations were evident in the inventories, despite a general downward trend, especially in the manufacturing sector (Berg 2016).

In Massachusetts, the discrepancy between NEI and TRI emissions is especially important. As Figure 1.3 shows, based on the 2014 NEI inventory most mercury releases in Massachusetts come from nonpoint rather than point sources, which are not included in the TRI data (US EPA 2019). In general, there is greater uncertainty in nonpoint sources as these are by definition small sources which are not measured directly.
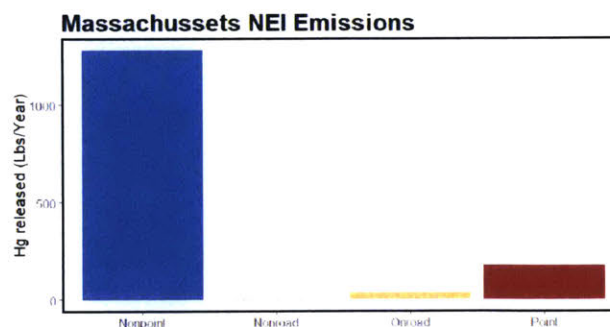

Fig. 1.3: The total nonpoint, onroad, offroad and point emissions included the the 2014 NEI inventory for Massachusetts

Globally, emissions inventories for point sources are usually derived via extrapolation of secondary information, such as data about industry sizes and assumptions about emissions, rather than direct measurements. Uncertainties and inconsistencies in extrapolation assumptions lead to large emission estimate uncertainties (Kwon and Selin

2016). North American emissions inventories utilized in global atmospheric models for UNEP assessments are estimated to have an uncertainty of -43/+129%, with especially high uncertainties for certain sectors such as cement production, waste disposal and metal production, at -62/+273%, -75/+245% and -58/+242% respectively (AMAP/UNEP 2015).

1.2.3 Modeling Mercury

Global atmospheric models provide a useful tool for estimating mercury emissions and predicting concentration exposures, but poor constraints on physical processes and a lack of field data limits the accuracy of models and leads to large uncertainties, thus limiting their ability to link sources to receptors (Kwon and Selin 2016). Multiple models are in use for global mercury assessments, each of which produces varying distributions of mercury deposition and concentrations (Kwon and Selin 2016); For the purpose of this study, the parameterizations utilized in the GEOS-Chem global atmospheric chemistry model were considered. GEOS-Chem computes atmospheric concentrations of pollutants based on emissions, deposition and chemistry in a 3D global grid with a maximum resolution of 0.625^o by 0.5^o by 72 levels and one hour (GEOS-Chem 2019).

Aside from previously discussed anthropogenic emission uncertainties, uncertainties in natural biogeochemical cycles, including oxidation/reduction, deposition and legacy re-emissions, pose a major challenge for modeling. Various studies have proposed oxidation pathways involving Br, OH, O_3, HO_2, Cl and I (Horowitz et al. 2017). GEOS-Chem implements oxidation as two step reactions between Hg^0 and Br or Cl, followed by a second step reaction involving Br, Cl or NO_2, and thus calculates the lifetime of Hg^0 against oxidation to be 2.7 months (Horowitz et al. 2017). Reduction of mercury has been proposed to take place in the aqueous phase, via reaction with acids (Pehkonen and Lin 1998). Further studies have shown that in-cloud photoreduction is necessary to balance relatively fast Br oxidation and allow models to match observed total atmospheric lifetimes for Hg (Shah et al. 2016). In GEOS-Chem reduction is implemented as aqueous-stage photoreduction, with a rate constant adjusted so model results match observed atmospheric lifetimes (Horowitz et al. 2017).

Models agree that the contribution of legacy re-emissions to atmospheric Hg(0) concentrations is larger than direct anthropogenic emissions, but disagree on the exact fractions. Accurately modeling legacy re-emissions requires understanding both pre and post-industrial biogeochemical cycles, and deposition patterns (Kwon and Selin 2016). GEOS-Chem parameterizes soil re-emissions as a function of soil concentrations and short-wave radiation (GEOS-Chem 2019). Recent research by Khan et al. proposes to additionally include a sine-curve light variation function in the parameterization to better account for diurnal variations measured in the field. Model soil concentrations are based

on highly variable field measurements. For urban sites, soil concentrations have been found to range from 0.056 to 0.13 μg g^{-1}, with a median value of 0.088 μg g^{-1} (Eckley et al. 2016).

Ocean re-emissions in GEOS-Chem are constructed by spinning up the model from pre-industrial conditions to steady state and then introducing anthropogenic emissions. The model uses an ocean-slab representation, with a seasonally-varying mixed layer depth. The parameterization includes dark and light oxidation and reduction processes in the mixed layer, exchange with the deep ocean, and air-sea exchange comprised of deposition and wind-driven evasion (Soerensen et al. 2010). A lack of measurements and experimental data leads to uncertainties in model representations of complex ocean chemistry. Further, little data exists to verify the accuracy of open-ocean kinetics (Kwon and Selin 2016). Global inverse modeling suggests uncertainties in modeled ocean re-emissions of $\pm 63\%$ (Song et al. 2015).

GEOS-Chem dry deposition velocities are calculated according to a resistance-based model which includes aerodynamic, canopy, stomatal, cuticle uptake and soil resistance parameters (Zhang et al. 2003). This model calculates Hg^0 deposition velocities of 0.01 cm s^{-1} over water, 0.06 cm s^{-1} over urban areas, and 0.1 to 0.18 cm s^{-1} over forested regions (Zhang et al. 2009). By comparison, experimental studies have found deposition values over forested regions ranging from 0.0004 to 0.55 cm s^{-1} depending on the vegetation type, time of year, and site contamination (Zhang et al. 2009).

1.3 Previous Literature

Several previous studies have aimed provide insight into the uncertainties in biogeochemical mercury cycling and served as a starting point for this study. Studies of individual sites and collection of empirical data can provide information on local mercury concentration trends and cycling which may inform and be used as verification for more complex models, and further the understanding of global cycles.

Previous studies in New England have provided insight into local mercury cycling and emissions at specific sites but left some uncertainty as to whether these results generalize across the region. Lee et al (2001) found a strong correlation between Hg^0 and CO$_2$ concentrations in the northeastern US and from this ratio calculated an annual anthropogenic regional flux of Hg^0 of 41 +/-2 g/km^2/yr, with higher fluxes on clear, sunny days. This study suggests similar sources and cycling for CO$_2$ and mercury. However, the most recent NEI inventory lists the emission rate in Massachusetts at 29 g/km^2/yr (US EPA 2018) and several important regulations have come into play since the study was

performed in 2001, warranting further investigation into the New England mercury cycle now.

Records in New Hampshire found atmospheric concentrations of Hg^0 as well as oceanic tracers to be enhanced following strong springtime nor'easters, suggesting enhanced oceanic outgassing to be a major source (Sigler et al 2009). The North Atlantic is the one region of the ocean which is a net source rather than net sink for mercury, due to the large amount of legacy deposits resulting from high anthropogenic emissions in Europe and North America and slow oceanic mixing (Soerensen et al. 2010). In coastal New England, oceanic re-emissions could be an especially important component in the local mercury cycle and a major contributor to Hg^0 concentrations. Further studies are needed however, to understand this effect beyond individual large storm events.

Additional studies have attempted to understand mercury cycling in a specifically urban setting. Studies in Reno, Nevada and Dartmouth, Nova Scotia found strong diurnal and seasonal cycles in atmospheric mercury concentrations exist in urban environments as well as at background sites (Cheng et al 2014, Stamenkovic et al 2007). Stamenkovic et al. observed concentration peaks of total gaseous mercury in winter and spring, and a low point in summer, as well as a daily cycle with peaks in the morning and a minimum in the afternoon in Reno. Cheng et al observed similar cycles in both urban and rural sites in Nova Scotia, as well as influence from oceanic air masses on gaseous elemental mercury concentrations. This suggests similar processes control the cycling of mercury in both urban and rural locations, and follow-up studies on additional urban sites may shed light on the details of those processes.

Denzler et al (2018) found that a simple box model could capture diurnal cycles in an urban setting, during periods of strong atmospheric inversions in Zurich Switzerland, taking into account only flux in and out of the box and variations in the boundary layer height. This box model allowed for calculations of the urban anthropogenic emissions. The study demonstrated the ability of a relatively simple single box model to capture Hg^0 concentrations in a localized, urban setting. It also demonstrated that boundary layer fluctuations likely play a large role in regulating the hour to hour variations in observed concentrations. Such methodologies can be applied to other urban sites, with adjustments made to account for local meteorology and sources, in order to better understand local Hg^0 cycling.

1.4 Problem Statement

Currently, there are many uncertainties in mercury emissions and very little data on the efficacy of recent regulations in mitigating mercury pollution in the United States to

verify the outcomes predicted by models (Giang and Selin 2016). This study seeks to contribute to and improve on the existing body of knowledge regarding mercury cycling and emissions in the United States by providing an additional record of gaseous mercury concentrations in Boston, MA.

Boston provides an ideal study site due to it's coastal location, lack of large local mercury point sources, and position downwind of distant point sources to the west. Due to this positioning, local Hg^0 concentrations could potentially be impacted by both the long-distance transport of pollution plumes from out-of-state point sources and oceanic re-emissions. Thus, the site was chosen to provide insight into the relative effect of legacy re-emissions from the ocean compared to pollution dispersion from large anthropogenic sources and the biogeochemical cycling of Hg^0 in a coastal urban environment. Additionally, the site is geographically near several other sites previously studied, and can provide a reasonable point of comparison for attempting to understand how Hg^0 concentrations have changed since the implementation of new mercury regulations in 2015 (US EPA 2018).

By analyzing the record of Hg^0 concentrations in Boston, MA in conjecture with supplementary and historical data this study seeks to address the following questions:

- Understanding the long term, seasonal, and daily trends in Hg^0 concentrations in a coastal, urban environment, using Boston, MA as a case study.

- Identify likely major sources of mercury emissions contributing to observed pollution in Boston and understand the relative role of direct anthropogenic emissions vs. re-emission of legacy deposits.

- Provide an estimate of Boston area anthropogenic and oceanic emissions and understand how anthropogenic emissions have varied over time and how major inventories compare to model predictions.

Accurately understanding the amount and location of mercury emissions is crucial for crafting effective policy. This study aims to contribute to the body of knowledge regarding mercury emissions by reporting on a coastal, urban setting subject to inputs from both anthropogenic and oceanic reservoirs.

14

Methods 2

A record of Hg^0 was collected in Boston, MA from August 2017 to September 2018. The record was compared against supplementary meteorological and other air pollutant data, as well as previous records of Hg^0 from additional sites in North America. Potential source contribution function analysis was utilized to identify likely major sources of Hg^0 to the Boston area. A box model respresenting Boston was built and used to understand the sensitivity of Hg^0 concentrations to a variety of factors and estimate emissions.

2.1 Data Collection

Using a Tekran 2357A Ambient Air Analyzer, atmospheric concentrations of gaseous elemental mercury were recorded for 1 year (August 2017 to September 2018) on the roof of the College of Arts and Sciences building on the campus of Boston University (See Figure 2.1). Tekran 2357 instruments are commonly used at monitoring sites around the world for measuring atmospheric Hg^0 concentrations (Sprovieri et al. 2016). Integrated samples were analyzed every 15 minutes, and hourly averages were computed. In addition, Millipore 0.45 um cation-exchange membranes placed on the air inlet to the instrument collected divalent Hg species over two week periods and select filters were analyzed to determine the total divalent Hg concentrations. The air inlet was placed at approx. 1.5 meters above the roof, located 29 m above the ground at 45.3501 N, 71.1041 W, near the center of the Boston metro area. 15 m of Teflon tubing connected the air intake to the Tekran instrument. The Tekran has an error of 10% (Slemr et al. 2015).

An automatic calibration step of the Tekran instrument was carried out every 25 hours with an internal Hg permeation source. The accuracy of this permeation source was

checked against manual injections of saturated Hg vapor using a Tekran 2505 mercury vapor calibration unit and a Hamilton digital syringe, and following a strict procedure adapted from Dumarey et al. (1985), at the beginning and end of the one-year period reported here. Additionally, the National Atmospheric Deposition Program Atmospheric Mercury Network (NADP AMNet) standard operating procedure was thoroughly followed. AMNet aims to provide high quality, standardised records of atmospheric mercury concentrations from sites across the US (Atmospheric Mercury Network). Each site consists of a tekran checked at least biweekly, and each instrument is maintained to ensure compliance with standard allowed voltage, baseline deviation, sensitivity and argon gas flow ranges (AMNet Site Operations Manual). Screening criteria for data validation/invalidation were inspired by standard operative protocols used by AMNet, the Canadian Atmospheric Mercury Measurement Network (CAMNet) and the Global Mercury Observation System (GMOS).

2.2 Supplementary Data

Supplementary data was provided by researchers at Harvard University and Boston University, and by the Massachusets Department of Environmental Protection. Carbon dioxide and methane were recorded every 5 minutes at the same site at Boston University, and hourly averages were calculated from the quality controlled data. In addition, carbon dioxide, methane, and carbon monoxide were recorded at a Back Bay site, located approximately 1.5 miles east of the Boston University site (See Figure 2.1), at a height of

Fig. 2.1: The location of all sampling sites for pollutant data utilized in this study. Hg^0 was monitored at Boston university and supplementary pollutant data was collected at Boston University, Back Bay, and Kenmore Square.

228 meters (Sargent et al. 2018; Wofsy-Munger Group on Biosphere-Atmosphere Exchange 2019). Five minute measurements were recorded here as well, and averaged to obtain hourly values. Sulfur Dioxide data was obtained from the Massachusetts Department of Environmental Protection air quality station located in Kenmore Square, 250 meters east of the Boston University site (See Figure 2.1). Quality controlled SO_2 measurements were available for a limited time period, from August 2017 through December 2017, and were recorded hourly using UV fluorescence methodology (MassDEP 2019).
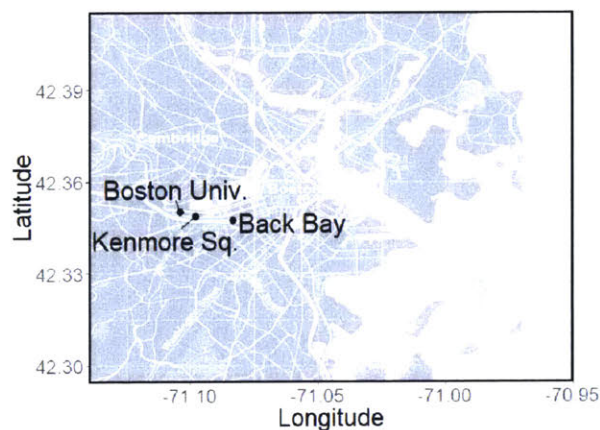
Meteorological data was extrapolated from grids produced by NOAA's High Resolution Rapid Refresh (HRRR) model (High Resolution Rapid Refresh 2019). The HRRR model has a spatial resolution of 3 km and is run every hour using radar data incorporated every 15 minutes, providing hourly data points for wind speed, direction, temperature, precipitation, humidity, snow cover, radiation and boundary layer height (Alexander et al. 2018). Observed meteorological data was available from Boston-Logan International Airport, situated 5 miles east of the Boston University site; however, the site for the observed meteorological data was prone to influence from sea-breeze fronts, and thus likely not always representative of conditions at the Boston University site. I compared the observed Logan Airport data to the HRRR data extrapolated at the airport and determined the two sources were consistent at this point, and so assumed the HRRR data provided a reasonable representation of actual meteorological conditions in the region. As the HRRR data provided better spatial resolution and data points nearer the Boston University site, it was utilized as the source for meteorological data.

Additional data from Hg^0 monitoring stations across North America were consolidated to compare against the Boston data. Their locations are shown in Figure 2.2. These stations are part of the Atmospheric Mercury Network (AMNet). At each site, a Tekran
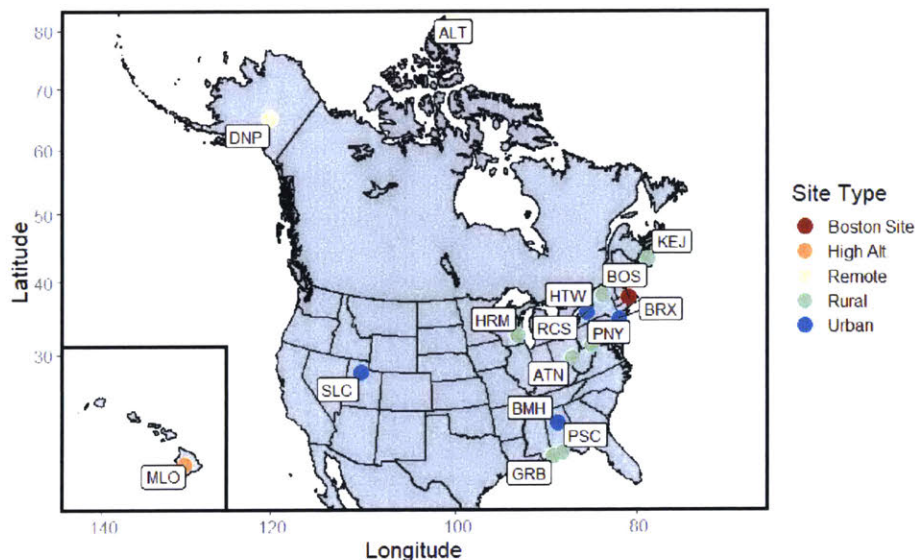
Fig. 2.2: A map of the AMNet stations in North America comprising the 2013-14 data set and the site type as classified by Gay et al. 2013. The full site names are as follows: MLO-Mauna Loa; DNP-Denali National Park; SLC-Salt Lake City; ALT-Alert, Canada; HRM-Horicon Marsh; GRB-Grand Bay; PSC-Pensacola; BMH-Birmingham; ATN-Athens; RCS-Rochester; HTW-Huntington Wildlife Refuge; PNY-Piney Reservoir; BRX-Bronx, New York City; KEJ-Kejimkujik; BOS-Boston.

2537 mercury vaporizer instrument was utilized to collect 5-minute samples and reported hourly averages using the standard AMNet operating procedures previously described. Data was collected and quality controlled, and sites categorized for 2013-2014 (Gay et el. 2013), and monthly averages compared against the Boston site data.

2.3 Potential Source Contribution Function Analysis

To understand the spatial arrangement of Hg^0 sources, the potential source contribution function analysis method was used. Back trajectories were generated every hour for the data timeseries using the NOAA HYSPLIT model. HYSPLIT uses a hybrid eulerian and lagrangian approach to calculate the path of an air parcel to a receptor over a set period backwards or forwards in time (Air Resources Laboratory 2019). For each Hg^0 concentration data point, HYSPLIT was run backwards for 24 hours to determine the origin of the air parcel containing the given concentration.

To perform the partial source contribution function analysis, the trajectory region was divided into a grid of evenly spaced boxes. Each box was assigned a value given by equation 2.1

$$B_{ij} = \frac{N_{ij}}{M_{ij}} \tag{2.1}$$

where M_{ij} is the total number of back trajectories passing through a given grid square and N_{ij} is the number of trajectories passing through that grid square representing a data point for which the Hg^0 concentration was greater than the mean Hg^0 concentration for the entire study period. Further, each box value was weighted according to the number of trajectories passing through the box, in order to assign a high likelihood of above-average pollution to regions which more consistently and frequently are origins for high-pollution parcels. The weighting function is described in Han et al. (2005).

2.4 One-Box Model

2.4.1 Model Structure

A box model was developed to simulate the Hg^0 concentrations recorded during the study period, test the sensitivity of concentrations to various factors, and estimate land and ocean emissions. All inputs to the model are summarized in Table 2.1. The model consisted of a single box situated over the Boston area, with concentrations in the box, C_{box}, simulated by integrating equation 2.2 over time.

$$\frac{dC_{box}}{dt} = \frac{E_{soil}r^2 + E_{NEI}r^2 + F_{in} - F_{out} - L_{box} - D_{urban}}{hr^2} \tag{2.2}$$

In equation 2.1, C_{box} denotes the Hg^0 concentration in the box representing the Boston area, in ng m^{-3}. r is the length of one side of the box, in meters. E_{soil} is the rate of re-emission of legacy deposits from the soil in the box, in ng $^{-2}$ hr^{-1}. E_{NEI} is the rate in the box of anthropogenic emissions, calculated from the NEI inventory and given in terms of ng $^{-2}$ hr^{-1}. F_{in} denotes the flux into the box due to advection and conversely F_{out} is the amount of Hg^0 removed from the box due to advection at the time step, with both calculated in terms of ng hr^{-1}. L_{box} is the amount of Hg^0 removed from the box due to oxidation to Hg(II), in ng hr^{-1}. D_{urban} is the amount of Hg^0 removed from the box due to dry deposition in an urban environment. h is the height of the box, which is given in meters and is taken to be the height of the planetary boundary layer, which is variable over time. Thus, at each time step the change in mass in the box is divided by the volume of the box at that time point, based on the boundary layer data, in order to solve for the Hg^0 concentration in the box.

Chemical loss in the box, L_{box} is calculated at each time step according to equation 2.3:

$$L_{box} = k_L C_{box} h r^2 \tag{2.3}$$

k_L is a rate constant calculated as the inverse of the lifetime of Hg^0 against oxidation in the atmosphere (Horowitz et al. 2017). The total mass of Hg^0 in the box at a given time step is multiplied by this constant to calculate the amount of Hg^0 removed via oxidation at that time step.

The amount of Hg^0 removed via dry deposition is calculated at each time step according to equation 2.4:

$$D_{urban} = v_{urban} C_{box} r^2 \tag{2.4}$$

v_{urban} is the dry deposition velocity of Hg^0 over an urban region, as calculated by Zhang et al. (2009), in m hr^{-1}. This is mutliplied by the amount of Hg^0 per meter of height in the box to obtain the total mass removed for each time step.

E_{soil} was calculated using the procedure outlined in Khan et al. (in prep). Based on fitting to measurements of field flux data, Khan et al. proposes calculating soil emissions by equation 2.5:

$$E_{soil} = 10^{0.709 + 0.119 log(c_{soil}) + 0.137 log(R_g)} \frac{1}{a} sin\left(\frac{\pi n}{d}\right) \tag{2.5}$$

In this parameterization c_{soil} is the concentration of legacy Hg^0 in soils in mug g^{-1}. a is a constant. d is the duration between sunrise and sunset on the day in which the soil emissions are being calculated, and n is the time of daylight hours which have passed at

the time at which emissions are being calculated (n will be 0 during the night). R_g is a factor calculated according to equation 2.6:

$$R_g = SWRe^{-\alpha LAI} \tag{2.6}$$

SWR is the amount of downward shortwave radiation at the timestep. LAI is the leaf area index of foliage in the box, and α is a constant.

The flux out of the box is calculated according to equation 2.7. w is the wind speed, which is multiplied by the concentration in the box and the area of the box side through which advection is occuring to determine the total mass lost to advection.

$$F_{out} = C_{box}whr \tag{2.7}$$
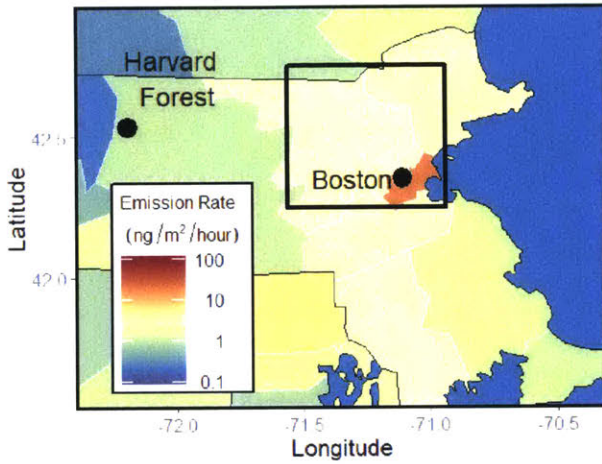
Fig. 2.3: The placement of the sampling stations at Harvard Forest and in Boston, relative to the GEOS-Chem box simulated in the model, defined by the GMAO 0.5° x 0.625° grid.

The flux into of the box was taken to be dependent on the direction of the wind. When winds were blowing from the east (when wind direction was between $30°$ and $210°$ from north) an "ocean flux in" was used, and when winds blew from the west, the opposing direction space, a "land flux in" was used. To obtain the land flux, additional Hg^0 measurements recorded at Harvard Forest, located in a rural part of Massachusetts, 90 km to the west of Boston, were averaged for each month in which the model was run and taken to be concentration, C_{landin}, for the flux into the box from the west. The ocean side flux in was calculated by solving the differential given in equation 2.8 for Hg^0 concentrations over the ocean (C_{ocean}), assuming concentrations were uniform across the ocean and $F_{in} = F_{out}$ for any arbitrary box drawn over the ocean contributing some flux in to the Boston concentrations:

$$\frac{dC_{ocean}}{dt} = \frac{E_{ocean} - D_{ocean}}{h} - L_{ocean} \tag{2.8}$$

20

E_{ocean} is the rate of legacy re-emissions from the ocean. D_{ocean} is the amount of mercury lost to deposition per unit area of ocean and L_{ocean} is the amount of mercury lost to chemical oxidation per unit area of the ocean. D_{ocean} is calculated in equation 2.9:

$$D_{ocean} = v_{ocean}C_{ocean} \tag{2.9}$$

where v_{ocean} is the deposition velocity over open water, in m hr^{-1}. Chemical loss L_{ocean} is calculated in equation 2.10:

$$L_{ocean} = k_L C_{ocean} \tag{2.10}$$

The various variable inputs to this model, the values utilized in the reference run of the model, and the sources for the values used are summarized in Table 2.1 below:

Variable	Name	Value	Units	Source
r	box side length	55000	meters	GEOS-Chem v11-02
h	boundary layer height	variable	meters	HRRR (NOAA)
E_{NEI}	anthropogenic emissions rate	4.19	ng/m^2/hr	NEI (EPA)
k_L	oxidation rate	0.00051	s^{-1}	Horowitz et al. (2017)
v_{urban}	urban deposition velocity	0.06	m/hr	Zhang et al. (2009)
C_{soil}	Hg^0 soil concentration	0.088	μg/g	Eckley et al. (2016)
a	soil constant	1.5	—-	Khan et al. (in prep)
d	# of daylight hours	variable	—-	—-
n	hour of daylight	variable	—-	—-
α	extinction coefficient	0.5	—-	Khan et al. (in prep)
LAI	leaf area index	variable	m^2/m^2	MODIS-Terra (NASA)
SWR	short wave radiation	variable	W/m^2	HRRR (NOAA)
w	wind speed	variable	m/hr	HRRR (NOAA)
C_{landin}	land concentration	variable	ng/m^3	Obrist et al.
E_{ocean}	ocean emissions rate	variable	ng/m^2/hr	GEOS-Chem v11-02
v_{ocean}	ocean deposition velocity	0.01	m/hr	Zhang et al. (2009)

Table 2.1: Summary of all variables and their values input into the one-box model

The box model area was defined to be the area covered by the box encompassing the Boston site in a GEOS-Chem grid. The model was run using the box defined by the GMAO 0.5^o x 0.625^o grid.

2.4.2 Emission Priors

The 2014 NEI emissions were utilized as a prior and point of comparison for non-soil terrestrial emissions in the model. Although the model was run for months in 2017 and 2018, the 2014 NEI emissions constituted the most recent and most complete inventory available. County emission rates were calculated by summing the 5 emissions types included in the inventory (point, nonpoint, onroad, nonroad, event) by county and dividing

by the area of the county (Figure 2.4). The emissions rate input into the model was a yearly rate calculated by averaging the county emission rates for all county areas contained within box model area.
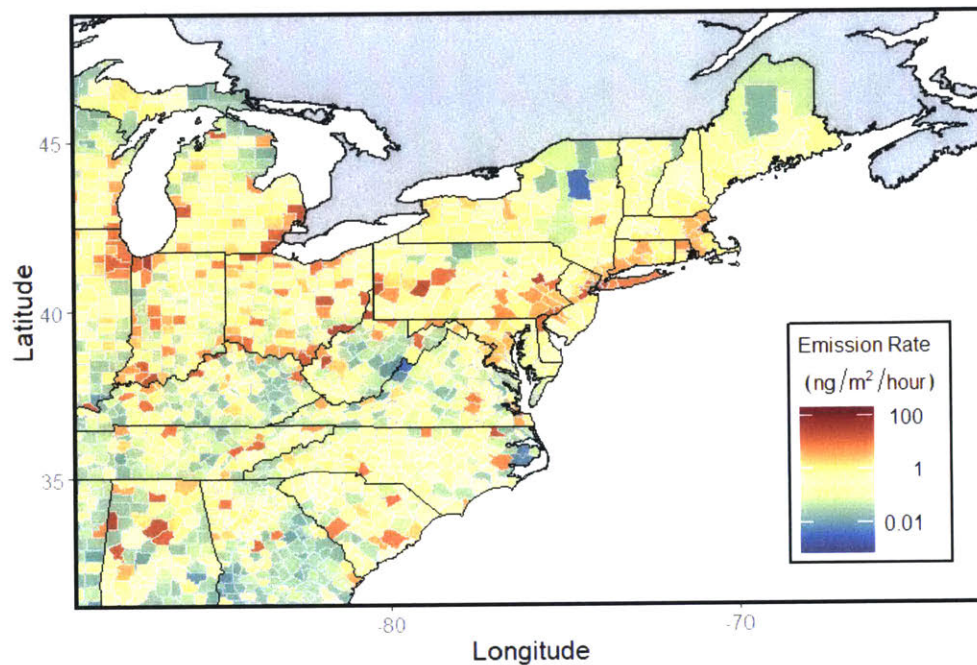

Fig. 2.4: The aggregated NEI 2014 mercury emissions, presented as a by-county emissions rate. The anthropogenic emissions prior for the model was then obtained by finding the area-weighted average of the emission rates for all counties contained within the model box.

Ocean emission priors for 2015 were obtained by calculating evasion fluxes from prescribed ocean concentrations utilized in the offline GEOS-Chem model and are shown in Figure 2.5 (Horowitz et al 2017; Zhang et al 2015). In the offline model, emission rates are calculated directly from constant ocean concentration estimates and meteorological data. Ocean circulation and dynamic air-ocean interaction effects on ocean concentrations are not included in the offline model. The emission rates for the box immediately to the east of Boston, which were given on a monthly basis, were taken to constitute the ocean emission prior in the one-box model (GEOS-Chem v11-02, UNEP 2018).

Several possible factors contributing to higher evasion in the North Atlantic are high mercury concentrations in the subsurface ocean layer due to high historical emissions from Europe and North America, enhanced Ekman pumping, and higher winds over the open ocean. High winter winds over the North Atlantic increase the mixed layer depth and thus drive increased enrichment of surface waters in Hg^0 from stores in subsurface waters. Near-shore emissions rates are lower possibly due to inaccuracies in model capture of mercury concentrations here and lower wind speeds. The offline GEOS-Chem model

does not include inputs from rivers which can be a significant source of mercury to the ocean in coastal environments (Soerensen et al. 2010).
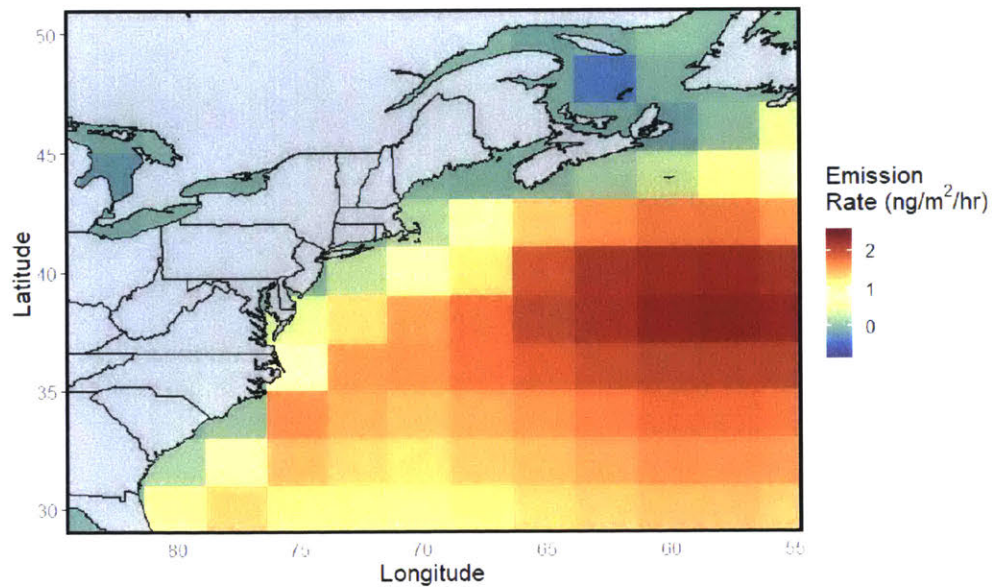
Fig. 2.5: The yearly average of the gridded monthly ocean emissions rates for 2015 calculated in the offline GEOS-Chem model from prescribed concentrations.

Results and Discussion 3

3.1 Hg^0 Concentration Comparison

The hourly averages of the Hg^0 data series recorded over the course of this study is shown in the top panel of Figure 3.1 below. The timeseries is characterized by day to day fluctuations and occasional large peaks which never exceeded 5 ng/m^3.
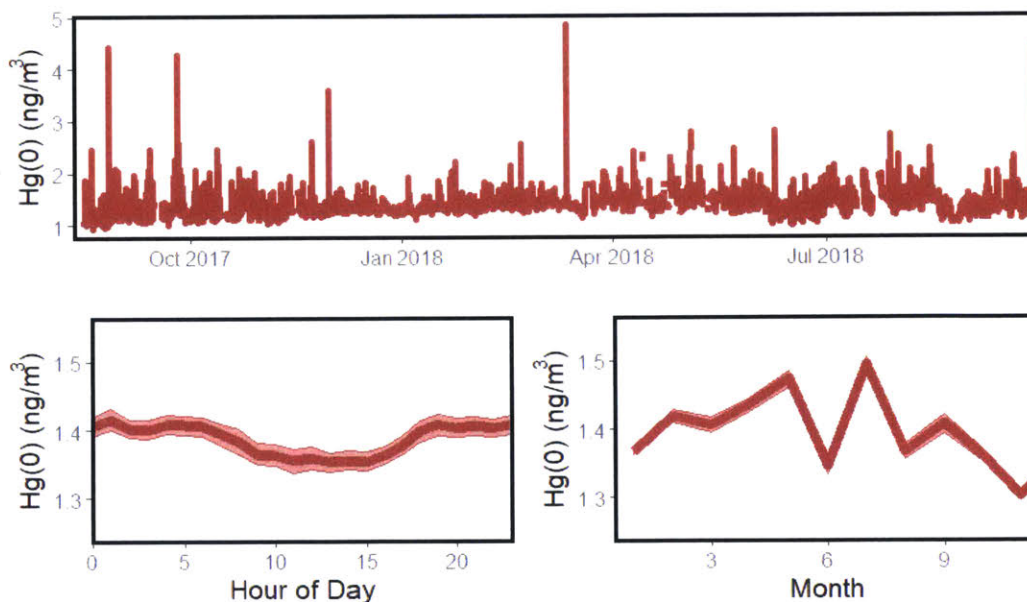
Fig. 3.1: (top) The hourly timeseries data recorded in Boston, MA during the study period. (bottom left) The diurnal cycle and 95% confidence interval in the Hg^0 data recorded in Boston, MA. (bottom right) The seasonal cycle and 95% confidence interval in the Hg^0 concentration data recorded in Boston, MA.

The average for all concentrations recorded at the Boston station was 1.38 ng/m^3 with a standard deviation of 0.21 ng/m^3. Hg^{II} concentrations recorded on the filters were extremely low, on average 16.3 pg/m^3, and so the analysis in this study focused on Hg^0.

In addition, the average daily Hg^0 concentration cycle (Figure 3.1, bottom left) and the average seasonal cycle (Figure 3.1, bottom right) are shown, along with the 95% confidence interval in the mean. The data displays a small diurnal cycle, with concentrations peaking at night and reaching a low in the afternoon on each day. This is consistent with the findings of previous studies (Cheng et al 2014, Stamenkovic et al 2007). The seasonal cycle shows generally higher concentrations in late winter and spring, and generally lower concentrations the rest of the year, reaching their lowest in November, which is also consistent with previous studies. The exception to this trend is July, during which average recorded Hg^0 concentrations were consistently above the long-term average.

In general, the diurnal cycle reflects meteorological changes throughout the day. As the sun rises in the morning it begins to heat the surface, increasing the height of the convective boundary layer. Hg^0 trapped near the surface during the night may circulate upward into a larger volume, decreasing overall concentrations. In addition, stronger convection during the day results in stronger winds which then more quickly remove Hg^0 which may build up in an urban area via advection. The diurnal trends in these meteorological variables in Boston is shown in the left column of Figure 3.2. This shows the trend in temperature, wind speed and boundary layer height is inversely related to the diurnal Hg^0 concentration cycle. Temperature, winds, and boundary layer height typically peak in midafternoon when Hg^0 concentrations are at a low.

The right column of Figure 3.2 shows the average seasonal cycle for boundary layer height, wind speed, and temperature. On this timescale, the cycle is not regulated by local heating and convection. Winter and spring, when temperatures are low and Hg^0 concentrations are increasing is generally characterized by well-ventilated conditions - a high boundary layer height and high wind speeds. Summer, when Hg^0 concentrations are generally lower (with the exception of July), is characterized by stagnant conditions - a low boundary layer and low wind speeds. These seasonal trends are likely the result of large scale rather than local meteorology. Strong hemispheric temperature gradients in northern hemisphere winter lead to stronger winds and less stagnant conditions. This suggests that other effects aside from the buildup of Hg^0 under a low boundary layer and stagnant conditions are responsible for regulating the seasonal Hg^0 trend.
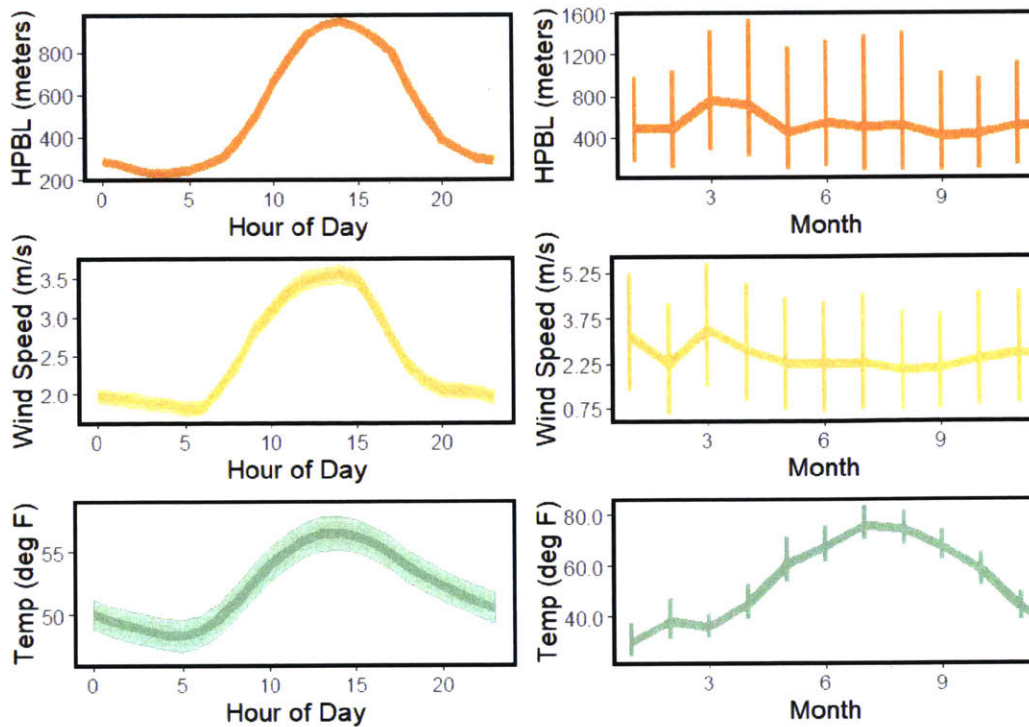
Fig. 3.2: (left column) The average diurnal cycle for the boundary layer height, wind speed and temperature in Boston, MA, along with the 95% confidence interval. (right column) The average seasonal cycle in boundary layer height, wind speed, and temperature in Boston, MA. The vertical lines show the average daily min and max in each month for the given variable.

To better understand long-term trends in Hg^0 concentrations, the Hg^0 concentrations collected at the Boston site from 2017-2018 were compared against data from sites across North America collected from 2013-2014 (bottom of Figure 3.3). They were compared to the 2014 NEI emissions data at each point for reference (top of Figure 3.3).

Boxplots of the monthly means for each site show that the Hg(0) concentrations measured in Boston in 2017-2018 are comparable to concentrations recorded at background sites in Hawaii, Alaska, and Nunavut in earlier years. Further, although Boston is an urban site, the concentrations observed are lower than those observed in all other urban sites in earlier years. By contrast, the emissions rate across all urban sites, including Boston, was comparable in the year 2014.
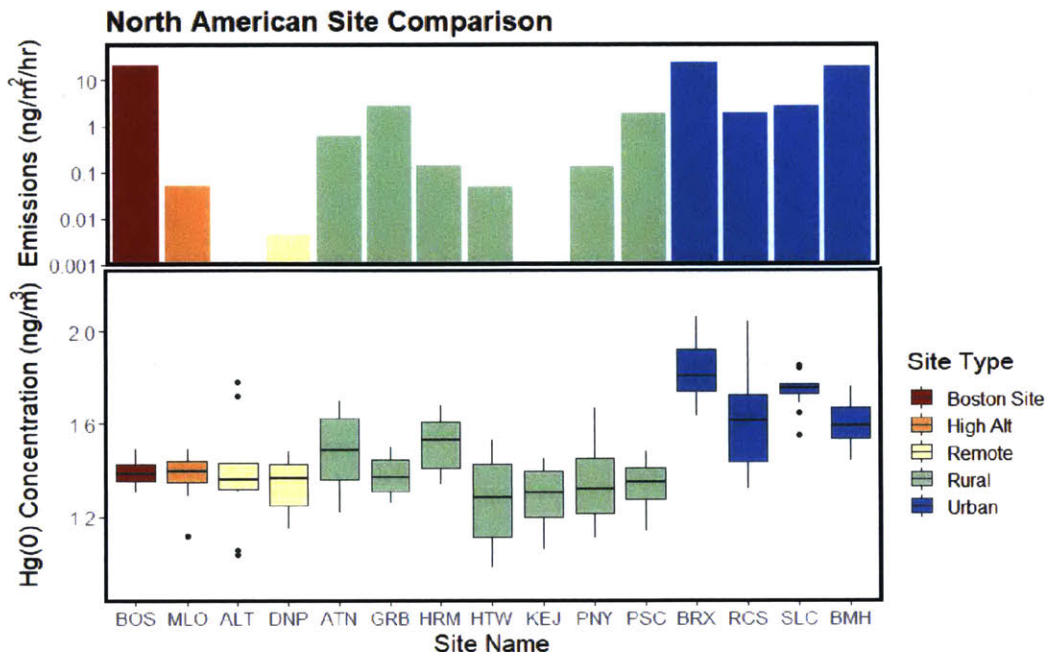
Fig. 3.3: (bottom) A box plot of monthly means for various sites in North America - see Figure 2.2 for the location of each site. (top) The emissions rate for the county in which each site is located, calculated from the 2014 NEI inventory. Note that emissions data is unavailable for Alert (ATL) and Kejimkujik (KEJ) as the NEI inventory only covers the United States.

By comparison, average Hg^0 concentrations at Harvard Forest, a rural site to the west of Boston, were 1.01 ng/m^3 in 2018, significantly lower than the remote sites included in the 2013-14 dataset. This implies that 2018 Hg^0 concentrations in not just Boston, but the larger region, are lower than many previously studied sites. Low concentrations in Boston and Harvard Forest compared to other similar sites could partially be due to the effect of plant uptake paired with few large local point sources. Massachusetts has significant tree cover, and plant uptake could decrease otherwise background concentrations leading to the relatively low observations. However, further research is needed to understand this possibility. Further, the concentrations in Boston and Harvard Forest, while low, do fall within the distribution of concentration levels for Northern Hemisphere sites as described in Sprovieri et al. (2016).

To better understand these observations, TRI emissions from 2014 (Figure 3.4) were compared to the most recent 2017 inventory (Figure 3.5).
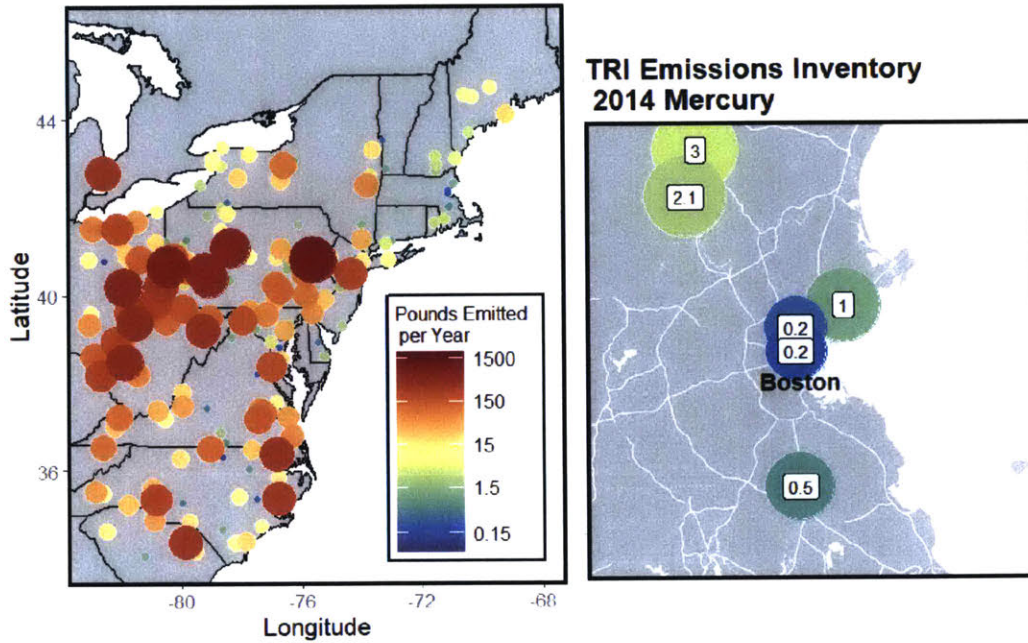
Fig. 3.4: 2014 TRI point source emissions. The left panel shows sources across the eastern US and the right panel shows the total emissions of point sources in the Boston metro area.
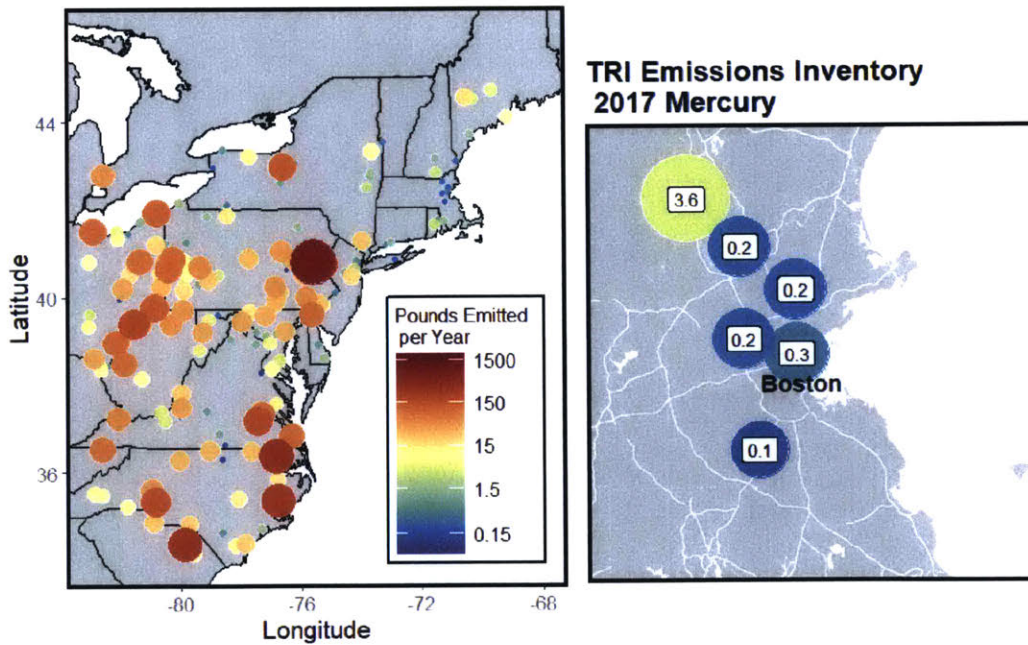
Fig. 3.5: 2017 TRI point source emissions. The left panel shows all sources in the eastern US and the right panel shows sources in the Boston metro area. There was a decrease in point source emissions from 2014 to 2017, particularly in West Virginia and Pennsylvania.

Although TRI does not include all sources covered by NEI, it is collected more frequently and can provide a sense of year to year changes in point source emissions.

The TRI data shows a marked decrease in emissions from point sources between 2014 and 2017. The decrease is especially pronounced for many coal-fired power plants in West Virginia and Pennsylvania, as well as for sources in New England. In the Boston metro area defined in Figure 3.4 and 3.5, point source emissions decreased from 7 lbs/yr in 2014 to 4.6 lbs/yr in 2017. This reduction in emissions may possibly explain the lower concentrations observed in Boston in 2017 compared to other urban sites in 2013-2014, although all sites had similar emissions in 2014.

Based on the supplementary site data in Figure 3.3, local emissions are not the only factor affecting relative observed Hg^0 concentrations. Several rural sites, such as GRB and PSC are located in counties with emissions rates at least an order of magnitude larger than the emissions rate at background sites. However, the concentrations observed at these sites were similar to observations at the background sites. This implies that higher local emissions does not necessarily translate to higher Hg^0 concentrations. Both these sites are coastal locations like Boston, and may be less susceptible to transport from anthropogenic sources due to frequent exposure to solely ocean-originating air masses.

By comparison, the high-concentration urban sources in Figure 3.3 are largely located away from the coast and thus subject to transport from non-local anthropogenic sources on all sides. The exception to this is the BRX site, which has a coastal location like Boston. However, Figure 3.4 and 3.5 show several large point sources directly to the east of BRX which may contribute to pollution transported to the site, whereas there are few point sources in the larger region (northern New England) in which Boston is located, thus making it less susceptible to regional transport.

All together, the supplementary site and emission data suggests several possible reasons as to why the Boston Hg^0 concentrations observed in 2017-2018 are comparable to background sites observed in 2013-2014 and less than other urban sites observed in 2013-2014. One possible reason is an overall decrease in emissions from 2014 to 2017, seen in the TRI inventory. In addition, the location of Boston, on the coast and in a region with fewer large point sources, may make it less susceptible to transport from outside the city itself. However, no long term records exist for Boston or the other sites to check the likelihood of these explanations or ascertain for sure if concentrations have actually trended downward in Boston or any other sites.

In order to better understand the likely sources for Hg^0 concentrations observed at the Boston site, the Hg^0 data was compared against supplementary data provided by Wofsky et al., Hutyra et al. and MassDEP for CO, CO_2, CH_4, and CO_2. The correlation between Hg^0 concentrations recorded at Boston University and all the supplementary

pollutant records is showed in Figure 3.6, along with the overall correlation coefficient between the timeseries.
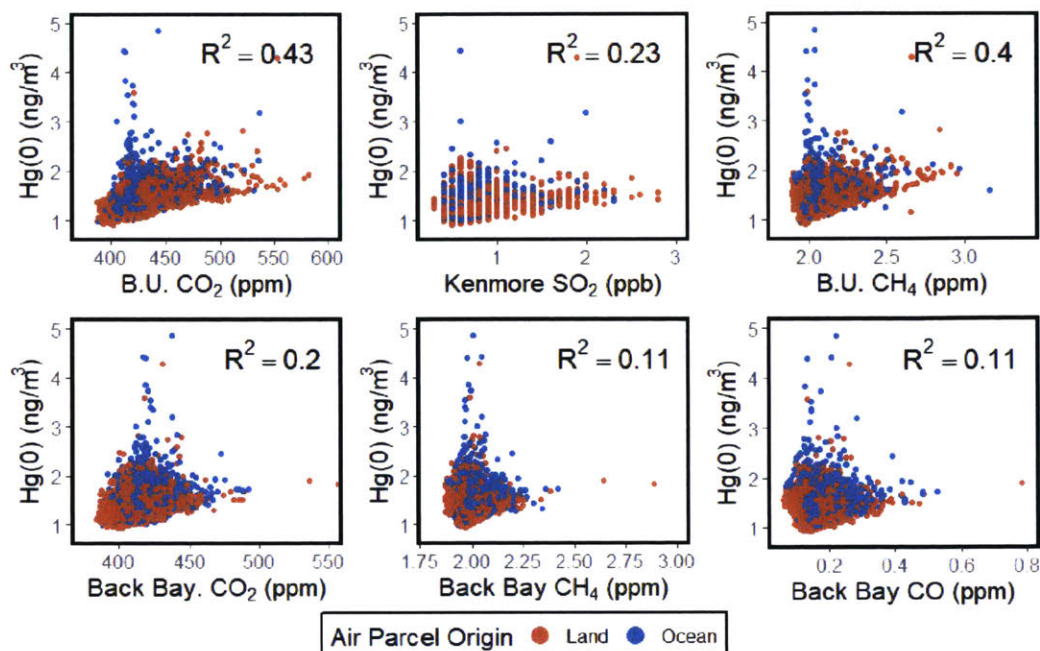

Fig. 3.6: Correlation plots between Hg(0) and supplementary pollutants collected during the same time period. Each point is colored according to whether it constitutes an air parcel originating from over ocean (a wind direction between $30^\circ N$ and $210^\circ N$) or over land (wind direction in the opposing direction). R^2 values for the data series are also given. Left to right across the top row are plots of the correlation between Hg^0 and CO_2 at Boston University, SO_2 at Kenmore Square, and CH_4 at Boston University. Left to right across the bottom row is the correlation with CO_2, CH_4 and CO at the Back Bay site.

In general, the overall correlation between additional pollutants and Hg^0 was very poor. The best correlation was with CO_2 measured at Boston University (Figure 3.6, top left) and CH_4 measured at Boston University (Figure 3.6, top right), the same location and height as the Hg^0 record. The correlations are further broken down in Table 3.1, which lists the correlation coefficients between Hg^0 concentrations and the supplementary pollutants measured in air parcels determined to be of a land origin (measured when wind direction was between $210^\circ N$ and $30^\circ N$), an ocean origin (measured when wind direction was between $30^\circ N$ and $210^\circ N$), and the overall correlation between the full timseries.

	B.U. CO_2	B.U. CH_4	Back Bay CO_2	Back Bay CH_4	Back Bay CO	SO_2
land	0.55	0.51	0.23	0.13	0.11	0.26
ocean	0.37	0.35	0.19	0.14	0.11	0.27
overall	0.43	0.4	0.2	0.11	0.11	0.23

Table 3.1: The R^2 correlation coefficients between Hg^0 concentrations and the concentrations of supplementary pollutants recorded in land-originating and ocean-originating air parcels, as well as the overall correlation between the full timeseries.

30

In general, Hg^0 was poorly correlated with the supplementary pollutants, whether considering land-originating or ocean originating air parcels. The best correlation was with CO_2 and CH_4 recorded at Boston University, at the same height and location as the Hg^0 concentrations, and this correlation was improved when only considering air parcels originating to the west, over land. Many anthropogenic sources which release Hg^0, such as coal fired power plants and other industrial facilities, also release large quantities of additional pollutants, especially CO_2 and SO_2. Further, as evidenced by the discrepancy in NEI and TRI emission totals in Figure 1.2, significant Hg^0 emissions come from general background onroad and offroad and nonpoint sources, which are more concentrated in urban areas, and also release significant CO_2, CH_4 and other pollutants.

The Boston University Hg^0, CO_2 and CH_4 concentrations were recorded in a dense urban area and only 25 meters off the ground. By comparison, the Back Bay records were taken at 228 meters, frequently above the planetary boundary layer, and thus far more prone to influence from long-distance transport of pollutants. The decent correlation between the Boston University records of CO_2 and CH_4, especially in land originating parcels, and Hg^0 paired with the poor correlation with measurements made at the Back Bay site suggests the Hg^0 concentrations recorded do not reflect influence from long distance transport of pollution. Rather, the Hg^0 concentrations recorded likely reflect input from local, general urban background sources as far as they are influenced by anthropogenic emissions. Further, the correlation between land-originating CO_2 and CH_4 and Hg^0 was somewhat better than for ocean originating parcels, but there was still some correlation in the ocean-originating parcels. Since there are minimal distant CO_2 and CH_4 sources across the open ocean, this further suggests that the concentrations observed at Boston University are reflective of local, background sources.

Hg(0) (ng/m^3)

In addition, Hg^0 concentrations are not particularly well correlated with the SO_2 record, which was recorded at ground level. Coal power plants are major sources for SO_2 and Hg^0, and so the lack of correlation between the two records suggests that coal power plant emissions did not have a large impact on the Hg^0 concentrations observed.

To better understand the relationship between Hg^0 and other crucial pollutants, pollution roses were plotted for the Hg^0 data (Figure 3.7) and each supplementary

Fig. 3.7: Hg^0 concentration pollution rose.

pollutant measured (Figure 3.8). These plots depict the concentration of each pollutant as a function of the wind speed and direction.
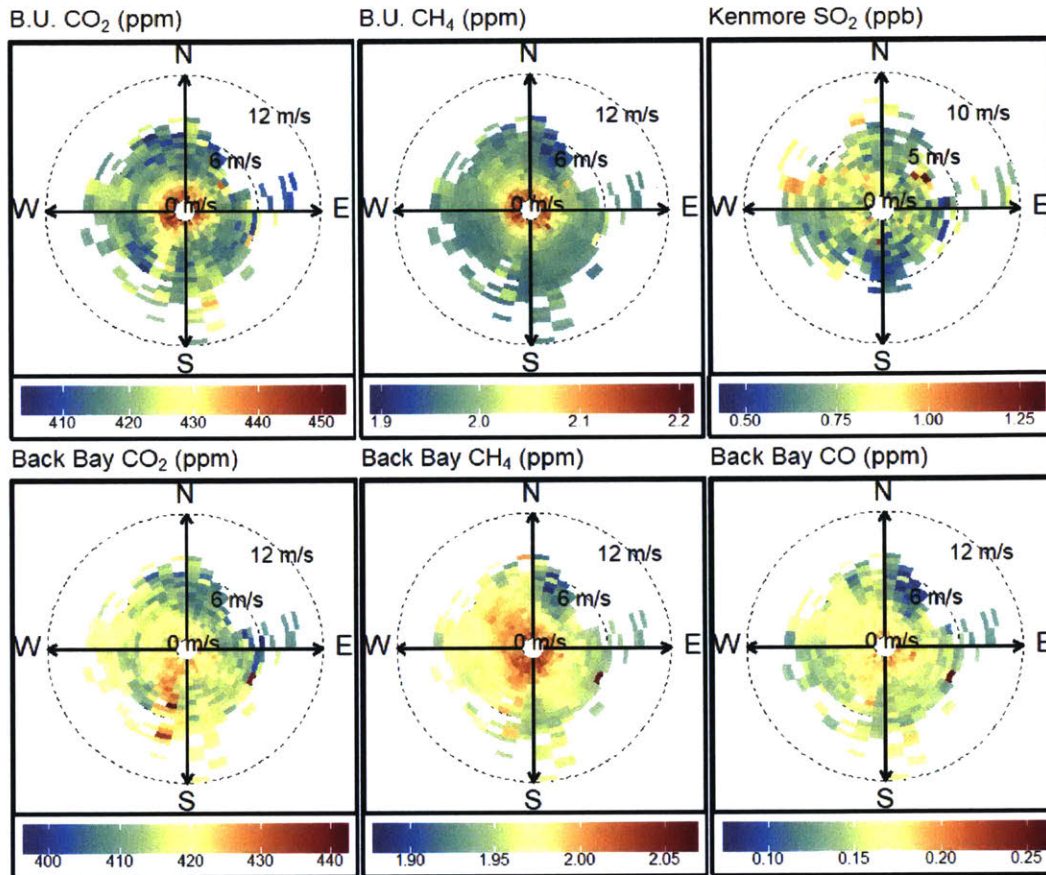
Fig. 3.8: Wind roses depicting the average concentration of each supplementary pollutant recorded coinciding with the full range of wind directions and speeds measured during the study period. From top left to bottom right the plots depict concentrations of CO_2 at Boston University, CH_4 at Boston University, SO_2 at Kenmore Square, CO_2 at Back Bay, CH_4 at Back Bay, and CO at Back Bay respectively.

The pollution roses in Figure 3.8 show that especially in the case of the records for CO_2 at Boston University (top left), CH_4 at Boston University (top center),and CH_4 at Back Bay (bottom center), concentrations are generally higher under low-wind, stagnant conditions, with no clear directionality. This further indicates local background sources are contributing to the buildup of these pollutants, as they tend to accumulate more under locally stagnant conditions, and there is no clear indicator of transport from elsewhere. By comparison, the Back Bay records of CO_2 (bottom left) and CH_4, which are more sensitive to long distance transport, show some indication of higher concentrations consistently coming from the southwest and northwest respectively, even under high-wind conditions, suggesting possible strongly influential sources in these directions. The pollution roses of SO_2 (top right) and CO (bottom right) show no clear patterns with regards to wind

conditions corresponding to high pollution events, indicating no one particularly strong source causes high pollution events.

By comparison, the pollution rose depicting average Hg^0 concentrations recorded at Boston University as a function of wind speed and direction (Figure 3.7) shows consistently higher Hg^0 concentrations when the wind direction is from the east, irregardless of the wind speed. This suggests a relatively strong source to the east of the measurement site, which is largely open ocean. Unlike as was observed for supplementary pollutants, the highest average Hg^0 concentrations were observed only in air parcels coming from the east, not in all directions under stagnant conditions, indicating general background urban pollution in fact plays less important of a role in regulating local Hg^0 concentrations compared to the role of the ocean to the east. In addition, the different patterns of the supplementary pollutants as a function of wind speed as compared to the pattern observed for Hg^0 indicates different emission sources contribute to high Hg^0 concentrations than the other pollutants measured. While the ocean is not a major source for CO_2, CH_4, SO_2 and CO, it can be a major source for re-emissions of Hg^0 (Obrist et al. 2018), and Figure 3.7 suggests this is the case in Boston.

3.2 Partial Source Contribution Function Analysis

In order to more rigorously identify likely geographical sources of observed gaseous Hg^0 concentrations, partial source contribution function (PSCF) analysis was performed. PSCF provides a useful tool for identifying regions in which it is likely high concentration plumes originate. The results of performing the PSCF analysis using the full timeseries of Hg^0 concentrations and the corresponding calculated back-trajectories is shown in Figure 3.9.

As the initial analysis of wind speeds and directions indicated, the PSCF analysis also shows that the region over the ocean to the east of Boston is a major source for Hg^0. This region has the highest likelihood of having had air parcels with Hg^0 greater than the mean pass over it. In general, most of the regions with a greater than 50% likelihood of having had air parcels with Hg^0 concentrations greater than the mean pass over them are located to the east and south of Boston, over the open ocean. By comparison, in general, most regions situated over land masses, where anthropogenic emission sources are located, have a less than 50% likelihood of having had an air parcel with Hg^0 concentrations above the mean pass through. Regions far from Boston, which were assigned lower PSCF likelihood by the weighting function due to having few trajectories pass through, generally still were assigned higher relative likelihoods over the ocean and lower likelihoods over land masses.
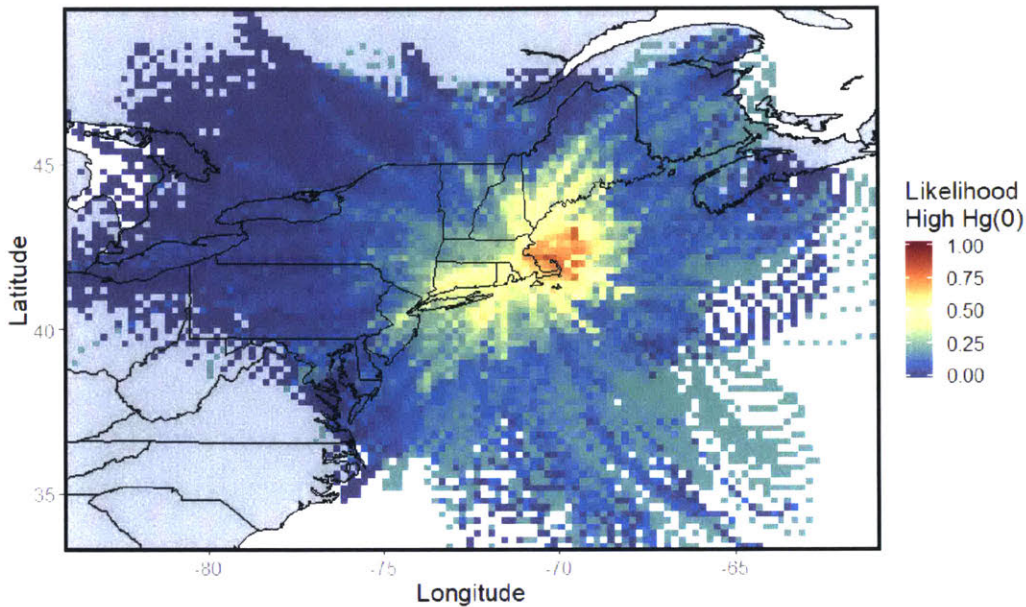
Fig. 3.9: Partial source contribution function analysis results for Hg^0 concentrations observed in Boston from 2017-2018.

Follow up analysis showed similar likely-source patterns continued to occur when only utilizing data for a single season, or for periods of a low boundary layer and stagnant conditions.

Similar analysis was performed to identify the likely sources of supplementary pollutants and compare against the likely Hg^0 sources. The PSCF analysis was performed using the full range of data available overlapping with the Hg^0 study period. For SO_2, thus PSCF analysis could only be performed utilizing data for 2017 due to the lack of quality data available for after December of 2017. For all other pollutants, the analysis utilized back trajectories from August 2017 to September 2018. The results of the PSCF analysis are shown in Figure 3.10.

Unlike in the analysis of the Hg^0 concentrations, the PSCF analysis of the supplementary pollutants showed likely sources mainly to the west, indicating an anthropogenic source. The regions with the highest likelihood of having had air parcels with high concentrations of CH_4, CO, and SO_2 passing over them were located over urban regions in New York and Connecticut, and to the north of Boston also over several urban centers in southern New Hampshire and Maine. The PSCF analysis performed with CO_2 timeseries showed a high likelihood for high CO_2 concentrations in air parcels arriving from the west, south, and north of Boston, passing over land masses.
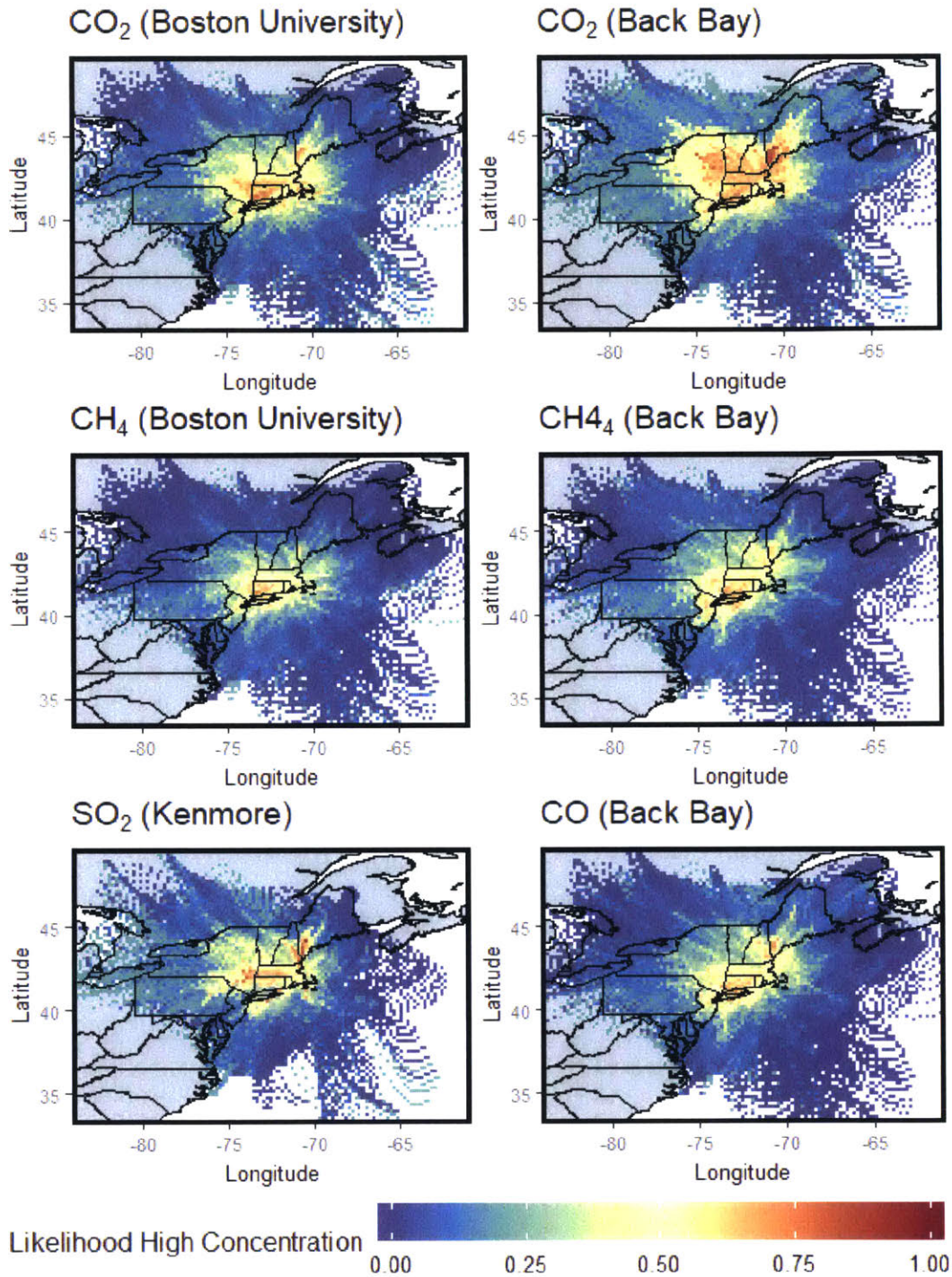
Fig. 3.10: Partial source contribution function analysis results for supplementary pollutants recorded in Boston, performed for all data in the study period. From top left to bottom right the PSCF analysis results are shown utilizing concentrations of CO_2 at Boston University, CO_2 at Back Bay, CH_4 at Boston University, CH_4 at Back Bay, SO_2 at Kenmore Square, and CO at Back Bay.

Follow up analysis showed similar likely-source patterns occurring in all seasons and meteorological conditions.

The PSCF analysis suggests that the main emission sources for Hg^0 are different from the main sources for supplementary pollutants observed in the Boston area. The main sources for the supplementary pollutants were likely anthropogenic in origin, with high pollution plumes originating over land masses west and south of Boston. Although potential anthropogenic sources for many of the supplementary pollutants, such as coal plants, other industrial point sources, and general background urban sources, can also be major sources of Hg^0, the PSCF analysis showed that these have a relatively minor influence on concentrations in Boston. Rather, legacy re-emissions from the ocean are a major source of Hg^0 input to the Boston region.

3.3 Box Model Results

The box model was utilized to estimate emissions for all months in 2018 and understand the sensitivity of concentrations to changes in various input parameters. For each month, the model was initialized with the first measured Hg^0 concentration of the month, and then run for the duration of the month, producing hourly estimates. A 24 hour lowess smoothing function was applied to the model output and the measured concentrations. This removed hour-to-hour noise in the dataseries, which the model was poorly designed to capture due to the size of the box and use of regionally derived variables. This allowed for more straighforward analysis of the diurnal and seasonal cycles, as well as changes due to wind direction variation occuring on multihour timescales.
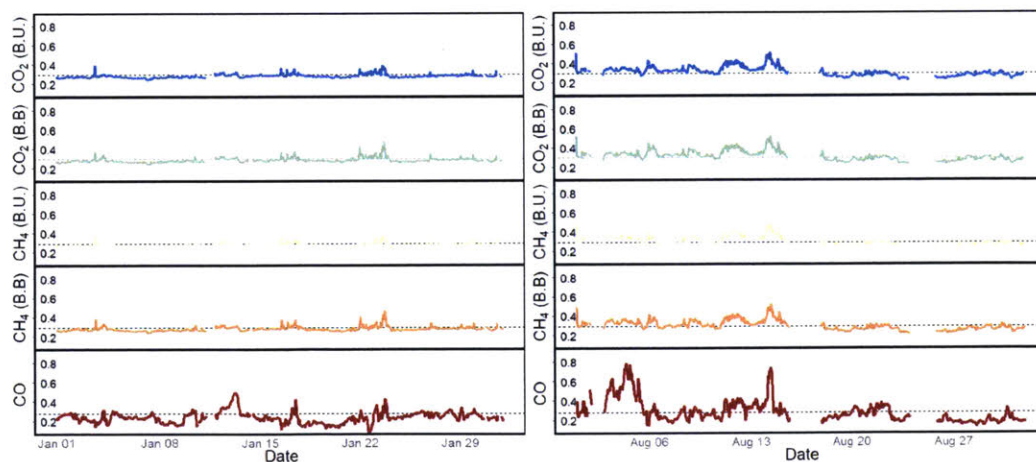
Fig. 3.11: The ratio of Hg^0 to the supplementary pollutants in January and August of 2018. The ratio is normalized to 1 and the average ratio represented with a dashed line to show periods in which the ratio of Hg^0 compared to other pollutants was higher or lower than average.

Two months were identified as periods of potential interest for the purpose of examining the sensitivity of the model, January and August. These two months were selected primarily in order to test the sensitivity in both the warm summer months and cold winter months, when different pathways in the mercury cycle are enhanced or dampened. Soil emissions and plant uptake are limited, and wind speeds and advection are generally higher, in January compared to August. In addition, January and August contained several alternating periods of high and low Hg^0 ratios compared to other pollutants (Figure 3.11), indicating variation in wind direction and likely source input over the month. Analysis of the back trajectories confirmed that January and August were subject to input of air parcels from several alternating directions and locations, making them excellent candidates for analyzing model sensitivity to the full range of variables input into the model.

To perform a sensitivity analysis of the model, a reference run was conducted using the assumed variable values taken from the literature and datasets, as given in Table 2.1. Then, sensitivity runs were conducted by varying each variable, one at a time by $\pm25\%$. The average percent change in the output concentrations from the reference run concentrations due to changing a given variable by $\pm25\%$ was reported for each variable. The results of this analysis, for sensitivity runs conducted on all variables in both January and August, are reported in Table 3.2.

Variable	January		August	
	+25%	-25%	+25%	-25%
LAI	-0.007%	+0.007%	-0.09%	+0.092%
α	-0.007%	+0.007%	-0.089%	+0.09%
C_{soil}	+0.045%	-0.056%	+0.18%	-0.22%
SWR	+0.05%	-0.6%	+0.21%	-0.26%
a	-0.18%	+0.19%	-0.59%	+0.97%
k	-0.48%	+0.51%	-0.90%	+0.94%
h	-0.94%	+1.54%	-0.95%	+1.81%
E_{ocean}	+1.08%	-1.07%	+2.71%	-2.71%
w	-1.21%	+1.85%	-1.78%	+2.86%
v_{water}	-1.31%	+1.58%	-3.51%	+4.31%
r	+1.40%	-1.52%	+2.16%	-2.23%
v_{urban}	-1.67%	+1.71%	-2.38%	+2.48%
E_{NEI}	+2.93%	-3.14%	+4.05%	-4.19%
C_{landin}	+18.83%	-18.78%	+13.15%	-13.30%

Table 3.2: The results of the sensitivity analysis conducted for the box model. The table values reported are the percent changes in the model output concentrations from a reference run due to changing the given variable by $\pm25\%$ from it's assumed value, when running the model for the given month. The model reference run is a run of the model for the given month with all variables set to their assumed values, the value reported in the literature or measured, as summarized in Table 2.1

The box model was largely insensitive to changes in most input variables. For the majority of variables, a change of $\pm 25\%$ resulted in a change of only a few percent or less in the output concentrations. The exception to this is C_{landin}, the concentrations measured at Harvard Forest used to calculate flux into the western side of the box. Changing this variable by $\pm 25\%$ led to changes in the ouput concentration of nearly the same magnitude. Thus, error in these measurements would introduce significant error into the model estimations. The Tekran instrument which recorded Hg^0 concentrations at Harvard Forest has an uncertainty of $\pm 10\%$ (Slemr et al. 2015). Further, C_{landin} was calculated on a monthly basis, from the monthly average of the Harvard Forest measurements. The standard deviation in each monthly dataseries ranges from 10-15% of the mean. Thus, 25% was taken to represent a reasonable upper bound on the potential error in C_{landin}, and the main likely source of error in the box model results. All error ranges in model outputs were thus calculated by varying C_{landin} by $\pm 25\%$ and recording the corresponding change in model output as the upper or lower bound.

Once the model sensitivity was understood, it was utilized to estimate adjusted anthropogenic and oceanic emissions for the Boston region within a reasonable degree of error($\pm 10\%$), to compare against the NEI 2014 and GEOS-Chem offline emission priors. The estimation was conducted by running the model each month, for a combination of oceanic and anthropogenic emission rates. For each run, a residual was calculated by finding the average of the absolute difference between each data point in the measured data series and the model output. The anthropogenic and oceanic emissions rate which together minimized the residual for a month were taken to be the best-guess adjusted emission rates for that month. The same process was repeated with C_{landin} adjusted to $\pm 25\%$ the measured values in order to get upper and lower bounds on the adjusted emissions estimates. Further, the emission estimate error was extended to the upper/lower bound found plus the difference between that estimated emissions and the next higher/lower emission rate checked. This accounted for the use of discrete emissions estimates in the best fit runs, which limited the number of emissions guesses for which the residual was actually calculated.

The adjusted oceanic emissions rates are given by month in Figure 3.12, along with the 2015 GEOS-Chem offline emission rates utilized as the prior in the model. In addition, the yearly average of the emission rates is shown for both the prior and adjusted emissions. In order to adjust the model to best fit the measured values, oceanic emissions were increased from a yearly average rate of 0.24 ng/m^2/hr to 0.63 ng/m^2/hr. This is consistent with recent work from Zhang et al. (2019) which found global net Hg^0 evasion to be 12% higher when using a more physically representative version of GEOS-Chem coupled to the MIT global ocean circulation model, as compared to the offline version of GEOS-Chem.

Oceanic Emissions Estimates
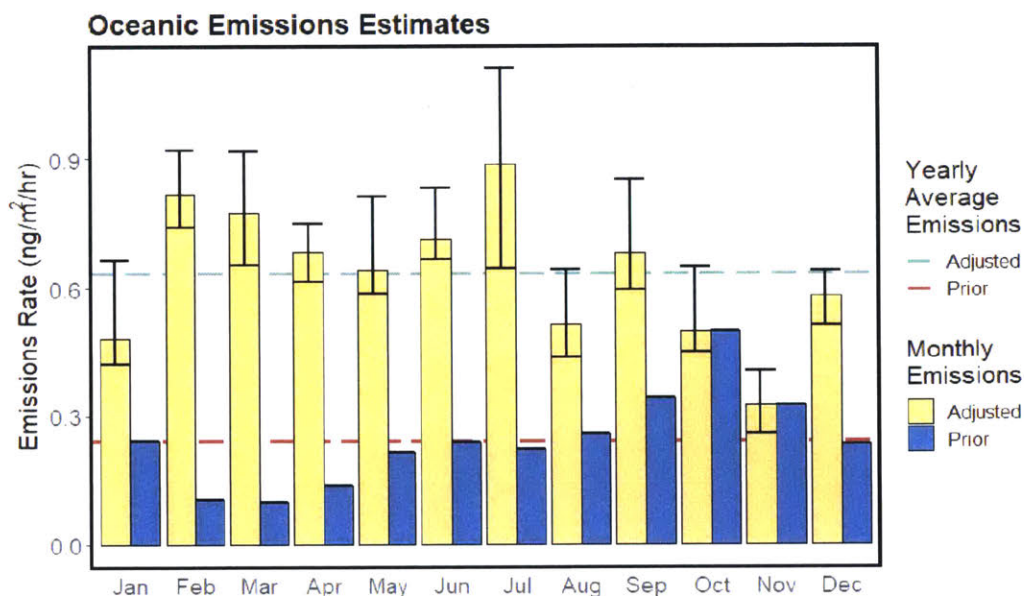
Fig. 3.12: Monthly adjusted ocean emission rates and error bars due to the uncertainty in input parameters for 2018, compared to the 2015 offline GEOS-Chem emission rates prior. In addition, the yearly means for both the adjusted and prior emission rates are given as a dashed line. Oceanic emission rates were approximately tripled from the prior in order for the box model results to best fit the concentrations recorded in Boston.

Further, the prior reflects a seasonal cycle in oceanic emissions, with emission rates peaking in late summer to fall, and at a low in spring. However, the results of the box model analysis suggest a different cycle is likely, with oceanic emissions peaking in late winter and again in summer after dropping a bit during late spring. There are several factors which may lead to this pattern in oceanic emissions. As seen in Figure 3.2, winds are generally stronger in late winter and spring, which may lead to increased evasion of Hg^0 from the ocean mixed layer during this time. In addition, the PSCF analysis (Figure 3.9) suggests a major source of Hg^0 to Boston is coastal waters immediately to the east of Boston. The offline GEOS-Chem emission priors (Figure 2.5) have a fairly coarse resolution of $4^o \times 5^o$, and thus can't capture very local effects. However, rivers and coastal upwelling are a localized source of Hg^0 to coastal regions (Cossa et al. 1996). In addition, higher deposition is expected near polluted urban regions. These additional inputs may result in higher oceanic concentrations of Hg^0 near coastal cities like Boston which are not captured in the offline priors, leading to the higher emission rates as predicted by the box model.

The adjusted anthropogenic emissions resulting from the best-guess box model runs are shown in Figure 3.13, as well as the reference emission rate prior derived from the NEI 2014 inventory. The NEI emissions rate is only given for the entire year due to the low time resolution of the dataset, but the model was adjusted for each month in order to

estimate monthly emissions rate and understand the seasonal cycle in emissions. Overall, the model predicted emissions were 61% higher than the prior. The model anthropogenic emissions rate estimate was 6.75 ng/m^2/hr compared to the emissions rate calculated for the box from the NEI prior of 4.18 ng/m^2/hr. In addition, the model results show a seasonal cycle in the anthropogenic emission rates, with emissions peaking in late winter and at a low in summer, with the exception of August, during which emissions peaked again.

The NEI emission inventory is expected to underpredict rather than overpredict emissions as it does not necessarily include every source in the Boston area. Biomass burning is known source of mercury; however, although the NEI inventory includes burning events, it did not report any mercury emissions in this category for the Boston area. Further, facilities are required to report emissions to NEI only if their emission potential is above a certain threshhold, and all smaller sources are estimated in the nonpoint category. This leaves the potential for underestimating small point sources. In Massachusetts, the majority of emissions are in the nonpoint category and are thus subject to higher uncertainty.

Anthropogenic Emissions Estimates
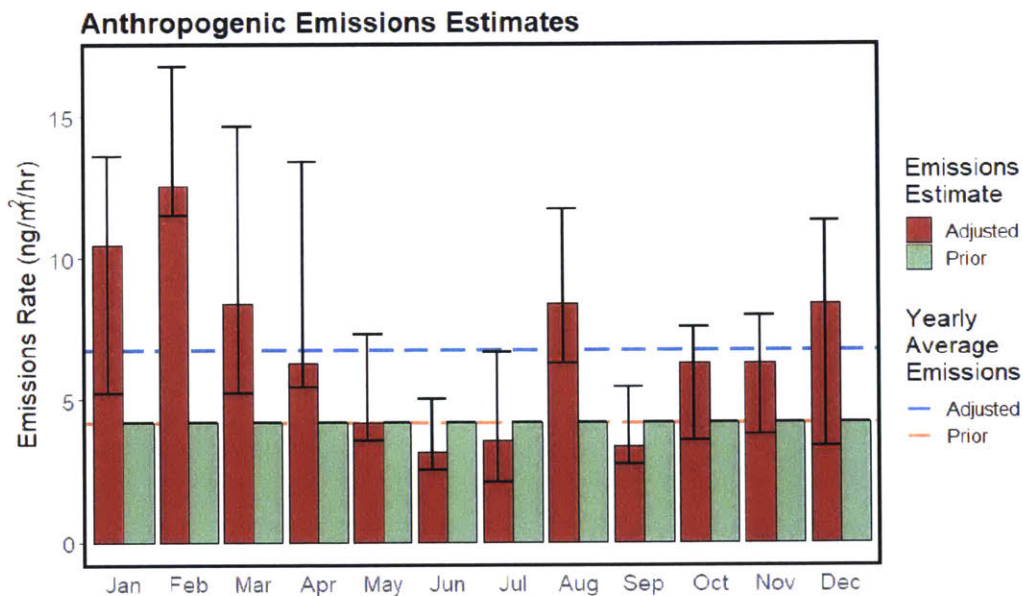
Fig. 3.13: Monthly adjusted anthropogenic emission rates as compared to the NEI 2014 emissions prior. The dashed line depict the yearly means of both the adjusted and prior emissions rates.

The seasonal cycle apparent in the model-adjusted emissions may be due to higher energy demands in winter and summer. Major sources for Hg^0 are energy generation facilities, especially coal plants, and so increased demand for energy, for heating in winter and cooling in summer, would impact emission rates. The apparent seasonal cycle may

also reflect trends due to plant uptake which is not accounted for in the model. During spring and summer, plants are able to remove additional Hg^0 from the atmosphere (Jiskra et al. 2018). If this effect was included in the model we would expect emission rates during these months to be higher to compensate for increased loss, and less of an apparent seasonal cycle in the anthropogenic emissions.

To examine the improvement from the adjusted emissions in the model's ability to accurately capture day-to-day trends in Hg^0 concentrations, the model output using both the prior and adjusted emissions with error due to error in C_{landin} is plotted alongside the measured concentrations in Figure 3.14.
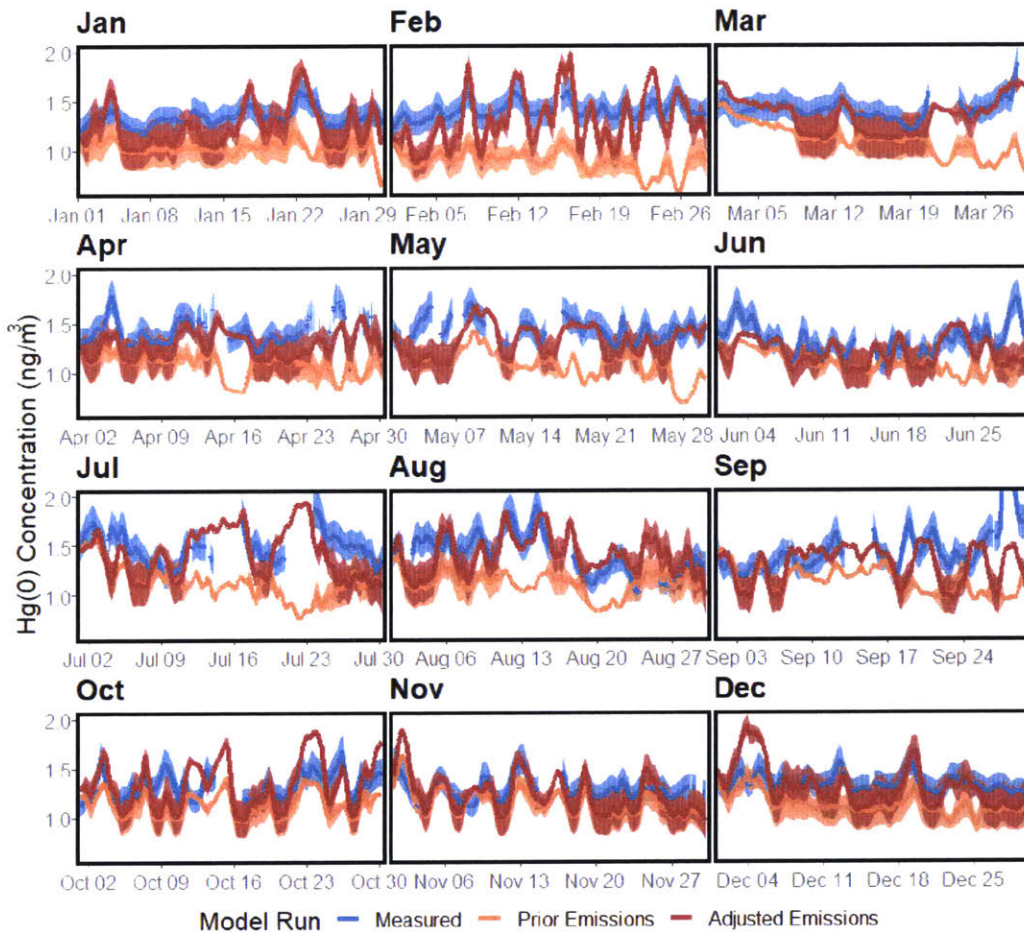
Fig. 3.14: The full smoothed timeseries of the Hg^0 concentrations measured in Boston with 10% error due to instrument error (blue), the results of the model run using the offline GEOS-Chem and NEI 2014 emission priors, with error due to the 25% error in C_{landin} values (orange), and the results of running the box model with the adjusted anthropogenic and ocean emissions, with error due to the C_{landin} error.

41

In general, the model, when run with the emission priors, tended to underestimate Hg^0 concentrations. The adjusted emissions provided nearer estimate to actual measured concentrations, more closely within the instrumentation error, and tended to also better capture the peaks and troughs in the Hg^0 concentration measurements. To better quantify this observation, the correlation coefficients and residuals between the measured data and the model output using both the prior and adjusted emission rates are given for each month in Table 3.3. The residual value is the average absolute difference between the measured concentrations and model output, as a percentage of the measured value.

Table 3.3: The correlation coefficients and residual values calculated for the measured Hg^0 concentrations and the model estimate. The model was run twice, using the prior emissions and the adjusted emissions, and the correlation coefficient and residual between each output and the measured concentration timeseries is given for each month in 2018.

	Prior Emissions		Adjusted Emissions	
	R^2	residual	R^2	residual
January	0.26	22.9%	0.87	10.9%
February	0.009	37.1%	0.82	13.7%
March	-0.06	19.4%	0.69	8.6%
April	-0.04	22.3%	0.71	10.7%
May	0.11	25.3%	0.46	9.2%
June	0.18	17.1%	0.27	11.1%
July	0.15	21.2%	0.36	14.3%
August	0.37	22.1%	0.53	10.9%
September	-0.37	22.3%	0.23	15.3%
October	0.38	15.2%	0.39	11.1%
November	0.55	12.4%	0.65	10.3%
December	0.43	16.6%	0.65	10.2%

In general, the model estimates from the prior emission rates were very poorly correlated with the actual measured data, and the residuals ranged from approximately 12-40% of the total value, far outside the range of instrument error. This suggests the prior emissions provide a poor representation of actual conditions in Boston, and with the processes included in the model, cannot explain the observed day to day variation in Hg^0 concentrations. Correlation coefficients were much improved in model runs utilizing the adjusted emission rates, although correlation remained low particularly in the summer and fall months. In addition, residuals were reduced to 8-15% which is much closer to the range of error on the tekran instrument utilized for collecting measurements ($\pm 10\%$).

These results suggest that while the model provides a useful representation of mercury cycling in late fall through early spring, it is less representative of the processes occurring in late spring through fall. The model does not account for plant uptake of Hg^0 which is a relatively new phenomenon under study but may play a significant role during summer months. In addition, the model does not account for wet deposition or reduction

of Hg^{II}, which mainly occurs in the aqueous stage, as these effects were assumed to be minimal and data on Hg^{II} was limited. However, although precipitation in Boston is roughly constant throughout the year, humidity is generally higher in summer and fall. Possibly, scavenging of mercury by water droplets is enhanced during the warm, humid summer months, to a significant degree, and inclusion of reduction and wet deposition in the model would provide a more physical representation of processes during these months.
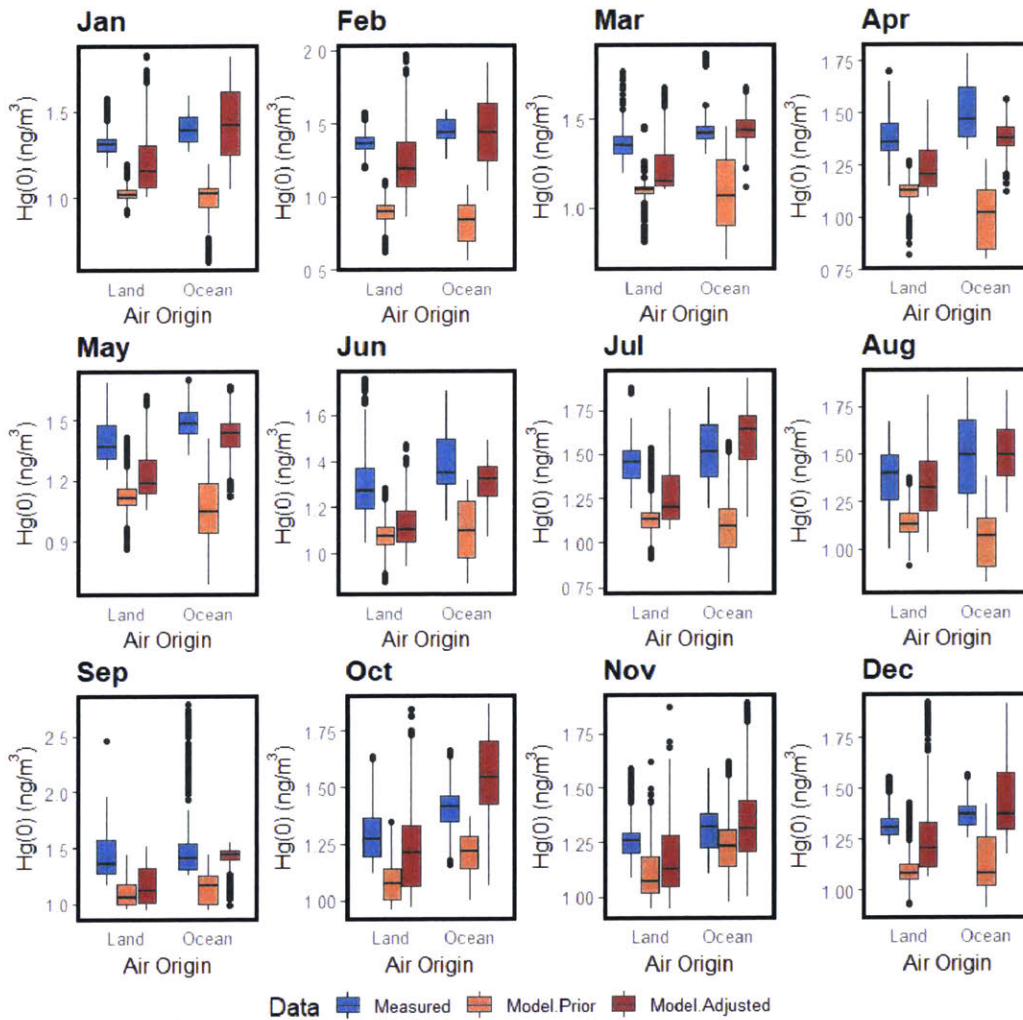
Fig. 3.15: Box plots for each month of land-originating and ocean-originating Hg^0 concentrations, for measured concentrations, concentrations predicted by the box model when run with the emissions priors, and concentrations predicted by the box model when run with the adjusted emissions.

Aside from providing a good overall match to the observed concentrations, specifically the longer day-to-day and seasonal trends seen in the smoothed data, another goal of the box model was to capture the effect of enhanced flux in from the ocean, on an

hour-to hour timescale. To test this, boxplots of Hg^0 concentrations in land and ocean originating air parcels are given in Figure 3.15 for the data series representing the measured concentrations, runs of the box model using the emissions priors, and runs of the box model using the adjusted emissions after minimizing the residuals.

In many months, the average Hg^0 concentration is slightly higher in air parcels originating from over the ocean (defined as measurements taken when wind direction was between 30^oN and 210^oN) compared to the land-originating parcels. The model results produced using the emission priors tended to not reproduce this effect, reporting equal means in air parcels originating from all directions, or slightly lower mean concentrations in ocean-originating air parcels. The adjusted emissions tended to improve the accuracy of the model in capturing this effect. Model runs with the adjusted emissions result in means for ocean-originating air parcels greater than those in land-originating air parcels, and nearly equal to the means reported in the measured data in most months. However, the model tends to still underestimate concentrations in land-originating air parcels.

While the reproduction of ocean-originating air parcel means lends some confidence to the adjusted ocean emission estimates, uncertainty remains due to the discrepancy in reproduced land-originating air parcel means from the measured values. One reason for this discrepancy may be the uncertainty in the Harvard Forest concentration mea-surements, which contribute directly to the flux in to the box on the land-originating side and to which the model is most sensitive. Figure 3.15 suggests that the flux into the box during periods of winds arriving from the west should be higher, indicating that the given C_{landin} values are too low. This may partially be due to the distance between the Harvard Forest station and the edge of the box being modeled, which sits along a rural-urban concentration gradient. Due to the presence of additional urban areas and potential Hg^0 sources between Harvard Forest and the box edge, likely the Harvard Forest concentra-tion measurements are not perfectly representative of the actual concentration flux into the box. The box edge is nearer the urban center and likely the actual concentrations here are higher than at Harvard Forest, which results in the box model underestimating concentrations during times of flux in from this direction.

Overall, the box model provides concentration estimates in agreement with the measured concentrations, within the error of the tekran instrument. The adjusted ocean emissions accurately capture increased concentrations in the Boston area during times of wind flow from the east. This further confirms the importance of the ocean as a source of Hg^0 in a coastal environment such as Boston.

Conclusions 4

There are several key takeaways from this study. First of all, the seasonal and diurnal trends observed in mercury concentrations in Boston, MA provide an additional point of support to back up previous studies which have also observed such trends. Hg^0 concentrations are influenced by changes in meteorological factors on daily and seasonal time scales, and this is important to keep in mind when thinking about pollution exposure.

Large point sources play a less important role than expected in contributing to Hg^0 exposure in Boston, MA. Recent regulations have placed stricter limits on Hg^0 emissions, and since 2014 emissions in New England and the larger east coast of the United States have decreased, particularly from coal-fired power plants. At the same time, the Hg^0 concentrations recorded in Boston are lower than those measured in other urban areas in 2013-2014, suggesting new regulations have possibly aided a tangible improvement in air quality.

However, decreasing anthropogenic point emissions does not remove all contributions to Hg^0 concentrations. This study shows that re-emission of legacy deposits to the ocean is a major source of Hg^0 in the coastal city of Boston. The timescales on which the ocean circulates and Hg^0 burial in deep ocean sediments occurs are very long, and so this source will persist for a very long time. In the future it will be increasingly difficult to decrease Hg^0 concentrations further due to the influence of this largely-uncontrollable source.

This study shed light on the limitations of large global models for capturing localized effects at play in a coastal urban environment such as Boston. Based on the results of the box model analysis, the offline GEOS-Chem oceanic emissions are underestimated in the region near Boston. This may partially be due to the spatial coarseness of the

model, which leaves it unable to capture very local effects and possible enrichment of Hg^0 concentrations leading to higher evasion. Accurately capturing this effect is important when attempting to reproduce concentrations in a coastal environment like Boston where oceanic evasion is shown to have a major effect. Further, the results of the emission estimates conducted in this study support recent research which have found the offline GEOS-Chem estimates are too low, when compared against estimates obtained using a more physically-representative version of the model which includes ocean circulation. The anthropogenic emission estimates conducted with the model showed that emission inventories likely do not capture all emission sources, and that the poor time resolution leads to possibly missing important trends in emissions over the year.

The box model utilized in this study, which built on previous work from Denzler et al (2018), proved to be a useful tool for examining mercury cycling in the Boston area. In addition, this study showed that the simple box model could be adapted to work in more complex environments than those explored in Denzler et al., such as the coastal urban center of Boston, MA. A one box model provides a useful tool for examining emissions in a small urban area, and may provide insight on localized effects which coarser global models may miss.

4.1 Future Work

The results of this study point to several potential areas for future research. While the results of the Hg^0 measurements recorded in Boston, MA and the comparison against past measurements and emission inventories suggest a decrease in Hg^0 concentrations coinciding with the introduction of stricter regulations, no direct comparison could be made from the data available. Long-term monitoring of Hg^0 concentrations at a consistent site is necessary to draw strong conclusions about decreases over time. In addition, more complete analysis of the emissions inventories over time is necessary to quantify any decrease in emissions, if one exists, and understand the main drivers of those changes in emissions. This study simply provides preliminary evidence to motivate considering such effects.

Future refinement of the simple box model described and used in this study could improve it's accuracy and help address remaining uncertainties in the dominant processes driving mercury cycling in localized environments. While the box model predicted concentrations within a reasonable margin of the measured values in the winter and spring, it performed less well in summer and fall. Part of the reason for the discrepancy may be due to the exclusion of some physical processes important to the mercury cycle, such as wet deposition, reduction, and plant uptake. These processes, excluding plant uptake, are included in global models, and future work may incorporate these processes into the

simpler single box model. This could inform the importance of these processes in local, urban areas and improve the accuracy of the model for the entire year. In addition, an improved one box model could provide a useful tool for municipalities to estimate local emissions and identify major inputs to atmospheric concentrations of Hg^0.

In light of recent proposed changes to the Mercury and Air Toxics Standards in the United States, this study provides evidence for the benefits of stricter controls on emissions. Boston benefits from the lack of large point sources, as evidenced by the low concentrations observed. However, emissions in Boston are still likely higher than currently reported due to uncertainty in the nonpoint category, which accounts for the majority of emissions in Boston. Future work may examine the benefit of regulations to address sources in these categories, especially for regions which have already decreased point source emissions.

Bibliography

Air Resources Laboratory (2019). *HYSPLIT*. Version 2.

Alexander, Curtis, Steve Weygandt, Stan Benjamin, et al. (2018). „WRF-ARW Research to Operations Update: The Rapid-Refresh (RAP) version 4, High-Resolution Rapid Refresh (HRRR) version 3 and Convection-Allowing Ensemble Prediction". In: p. 34.

AMAP/UNEP, 2015. *Global Mercury Modelling: Update of Modelling Results in the Global Mercury Assessment 2013*. Arctic Monitoring and Assessment Programme, Oslo, Norway/UNEP Chemicals Branch, Geneva, Switzerland. iv + 32 pp., p. 36.

AMNet Site Operations Manual (2015). *National Atmospheric Deposition Program*.

Amos, Helen M., Daniel J. Jacob, David G. Streets, and Elsie M. Sunderland (2013). „Legacy impacts of all-time anthropogenic emissions on the global mercury cycle". In: *Global Biogeochemical Cycles* 27.2, pp. 410–421.

Angot, H., M. Barret, O. Magand, M. Ramonet, and A. Dommergue (2014). „A 2-year record of atmospheric mercury species at a background Southern Hemisphere station on Amsterdam Island". In: *Atmospheric Chemistry and Physics* 14.20, pp. 11461–11473.

Atmospheric Mercury Network (2019). URL: http://nadp.slh.wisc.edu/AMNet/ (visited on May 1, 2019).

Axelrad, Daniel A., David C. Bellinger, Louise M. Ryan, and Tracey J. Woodruff (2007). „Dose–Response Relationship of Prenatal Mercury Exposure and IQ: An Integrative Analysis of Epidemiologic Data". In: *Environmental Health Perspectives* 115.4, pp. 609–615.

A. Perlinger, J., N. R. Urban, A. Giang, et al. (2018). „Responses of deposition and bioaccumulation in the Great Lakes region to policy and other large-scale drivers of mercury emissions". In: *Environmental Science: Processes & Impacts* 20.1, pp. 195–209.

Berg, Elizabeth (2016). „Mercury Emissions Inventories in the Lake Superior States". Thesis. Massachusetts Institute of Technology.

Cheng, Irene, Leiming Zhang, Huiting Mao, et al. (2014). „Seasonal and diurnal patterns of speciated atmospheric mercury at a coastal-rural and a coastal-urban site". In: *Atmospheric Environment* 82, pp. 193–205.

Clarkson, Thomas W., Laszlo Magos, and Gary J. Myers (2003). „The Toxicology of Mercury — Current Exposures and Clinical Manifestations". In: *New England Journal of Medicine* 349.18, pp. 1731–1737.

Cossa, D., M. Coquery, C. Gobeil, and J.-M. Martin (1996). „Mercury Fluxes at the Ocean Margins". In: *Global and Regional Mercury Cycles: Sources, Fluxes and Mass Balances.* Ed. by Willy Baeyens, Ralf Ebinghaus, and Oleg Vasiliev. NATO ASI Series. Dordrecht: Springer Netherlands, pp. 229–247.

Crump, K. S., T. Kjellström, A. M. Shipp, A. Silvers, and A. Stewart (1998). „Influence of prenatal mercury exposure upon scholastic and psychological test performance: benchmark analysis of a New Zealand cohort". In: *Risk Analysis: An Official Publication of the Society for Risk Analysis* 18.6, pp. 701–713.

Davidson, P. W., G. J. Myers, C. Cox, et al. (1998). „Effects of prenatal and postnatal methylmercury exposure from fish consumption on neurodevelopment: outcomes at 66 months of age in the Seychelles Child Development Study". In: *JAMA* 280.8, pp. 701–707.

Denzler, B., C. Bogdal, C. Kern, et al. (2018). „Urban source term estimation for mercury using a boundary-layer budget method". In: *Atmos. Chem. Phys. Discuss.* 2018, pp. 1–17.

Dumarey, R., E. Temmerman, R. Adams, and J. Hoste (1985). „The accuracy of the vapour-injection calibration method for the determination of mercury by amalgamation/cold-vapour atomic absorption spectrometry". In: *Analytica Chimica Acta* 170, pp. 337–340.

Eagles-Smith, Collin A., Ellen K. Silbergeld, Niladri Basu, et al. (2018). „Modulators of mercury risk to wildlife and humans in the context of rapid global change". In: *Ambio* 47.2, pp. 170–197.

Eckley, Chris S., Mike T. Tate, Che-Jen Lin, et al. (2016). „Surface-air mercury fluxes across Western North America: A synthesis of spatial trends and controlling variables". In: *Science of The Total Environment* 568, pp. 651–665.

Faïn, Xavier, Christophe P. Ferrari, Aurélien Dommergue, et al. (2009). „Polar firn air reveals large-scale impact of anthropogenic mercury emissions during the 1970s". In: *Proceedings of the National Academy of Sciences* 106.38, pp. 16114–16119.

Gay, D. A., D. Schmeltz, E. Prestbo, et al. (2013). „The Atmospheric Mercury Network: measurement and initial examination of an ongoing atmospheric mercury record across North America". In: *Atmospheric Chemistry and Physics* 13.22, pp. 11339–11349.

GEOS-Chem 2019 (2019). Version 12.3.2.

Giang, Amanda and Noelle E. Selin (2016). „Benefits of mercury controls for the United States". In: *Proceedings of the National Academy of Sciences* 113.2, pp. 286–291.

Gibb, Herman and Keri Grace O'Leary (2014). „Mercury Exposure and Health Impacts among Individuals in the Artisanal and Small-Scale Gold Mining Community: A Comprehensive Review". In: *Environmental Health Perspectives* 122.7, pp. 667–672.

Grandjean, P., P. Weihe, R. F. White, et al. (1997). „Cognitive deficit in 7-year-old children with prenatal exposure to methylmercury". In: *Neurotoxicology and Teratology* 19.6, pp. 417–428.

Gustin, Mae Sexauer, Steven E Lindberg, Kenneth Austin, et al. (2000). „Assessing the contribution of natural sources to regional atmospheric mercury budgets". In: *Science of The Total Environment* 259.1, pp. 61–71.

Han, Young-Ji, Thomas M. Holsen, Philip K. Hopke, and Seung-Muk Yi (2005). „Comparison between Back-Trajectory Based Modeling and Lagrangian Backward Dispersion Modeling for Locating Sources of Reactive Gaseous Mercury". In: *Environmental Science & Technology* 39.6, pp. 1715–1723.

Harada, Masazumi (1995). „Minamata Disease: Methylmercury Poisoning in Japan Caused by Environmental Pollution". In: *Critical Reviews in Toxicology* 25.1, pp. 1–24.

High-Resolution Rapid Refresh (HRRR) (2019). URL: https://rapidrefresh.noaa.gov/hrrr/ (visited on May 19, 2019).

Horowitz, Hannah M., Daniel J. Jacob, Yanxu Zhang, et al. (2017). „A new mechanism for atmospheric mercury redox chemistry: implications for the global mercury budget". In: *Atmospheric Chemistry and Physics* 17.10, pp. 6353–6371.

Jensen, S. and A. Jernelöv (1969). „Biological Methylation of Mercury in Aquatic Organisms". In: *Nature* 223.5207, pp. 753–754.

Jiskra, Martin, Jeroen E. Sonke, Daniel Obrist, et al. (2018). „A vegetation control on seasonal variations in global atmospheric mercury concentrations". In: *Nature Geoscience* 11.4, pp. 244–250.

Khan, T.R., D Obrist, Y Agnan, and J.A. Perlinger. „Atmosphere-terrestrial exchange model parameterization of gaseous elemental mercury: sensitivity analyses and direct comparison to measured field data". In: *(in prep)*.

Kwon, Sae Yun and Noelle Selin (2016). „Uncertainties in Atmospheric Mercury Modeling for Policy Evaluation". In: *Current Pollution Reports* 2.

Lee, Xuhui, O. Russell Bullock, and Robert J. Andres. „Anthropogenic emission of mercury to the atmosphere in the northeast United States". In: *Geophysical Research Letters* 28.7, pp. 1231–1234.

MassDEP (2019). *MassAir Online.* URL: http://eeaonline.eea.state.ma.us/dep/massair/web/#/trends/site?siteid=22&pollutantcode=42401&calc=DM&period=1M (visited on May 19, 2019).

Myers, Gary J., Philip W. Davidson, Christopher Cox, et al. (2003). „Prenatal methylmercury exposure from ocean fish consumption in the Seychelles child development study". In: *Lancet (London, England)* 361.9370, pp. 1686–1692.

Obiri, Samuel, Philip O. Yeboah, Shiloh Osae, and Sam Adu-Kumi (2016). „Levels of arsenic, mercury, cadmium, copper, lead, zinc and manganese in serum and whole blood of resident adults from mining and non-mining communities in Ghana". In: *Environmental Science and Pollution Research* 23.16, pp. 16589–16597.

Obrist, Daniel, Jane L. Kirk, Lei Zhang, et al. (2018). „A review of global environmental mercury processes in response to human and natural perturbations: Changes of emissions, climate, and land use". In: *Ambio* 47.2, pp. 116–140.

Outridge, P. M., R. P. Mason, F. Wang, S. Guerrero, and L. E. Heimbürger-Boavida (2018). „Updated Global and Oceanic Mercury Budgets for the United Nations Global Mercury Assessment 2018". In: *Environmental Science & Technology* 52.20, pp. 11466–11477.

Pehkonen, Simo and Che-Jen Lin (1998). „Aqueous Photochemistry of Mercury with Organic Acids". In: *Journal of The Air & Waste Management Association - J AIR WASTE MANAGE ASSOC* 48, pp. 144–150.

Sargent, Maryann, Yanina Barrera, Thomas Nehrkorn, et al. (2018). „Anthropogenic and biogenic CO2 fluxes in the Boston urban region". In: *Proceedings of the National Academy of Sciences* 115.29, pp. 7491–7496.

Selin, Henrik, Susan Egan Keane, Shuxiao Wang, et al. (2018). „Linking science and policy to support the implementation of the Minamata Convention on Mercury". In: *Ambio* 47.2, pp. 198–215.

Selin, Noelle E. (2009). „Global Biogeochemical Cycling of Mercury: A Review". In: *Annual Review of Environment and Resources* 34.1, pp. 43–63.

Shah, V., L. Jaeglé, L. E. Gratz, et al. (2016). „Origin of oxidized mercury in the summertime free troposphere over the southeastern US". In: *Atmospheric Chemistry and Physics* 16.3, pp. 1511–1530.

Sigler, J. M., H. Mao, B. C. Sive, and R. Talbot (2009). „Oceanic influence on atmospheric mercury at coastal and inland sites: a springtime noreaster in New England". In: *Atmospheric Chemistry and Physics* 9.12, pp. 4023–4030.

Slemr, F., H. Angot, A. Dommergue, et al. (2015). „Comparison of mercury concentrations measured at several sites in the Southern Hemisphere". In: *Atmospheric Chemistry and Physics* 15.6, pp. 3125–3133.

Soerensen, Anne L., Elsie M. Sunderland, Christopher D. Holmes, et al. (2010). „An Improved Global Model for Air-Sea Exchange of Mercury: High Concentrations over the North Atlantic". In: *Environmental Science & Technology* 44.22, pp. 8574–8580.

Soerensen, Anne L., Daniel J. Jacob, Amina T. Schartup, et al. (2016). „A mass budget for mercury and methylmercury in the Arctic Ocean". In: *Global Biogeochemical Cycles* 30.4, pp. 560–575.

Song, S, Ne Selin, A L Soerensen, Hélène Angot, and R Artz (2015). „Top-down constraints on atmospheric mercury emissions and implications for global biogeochemical cycling". In: *Atmos. Chem. Phys.* P. 24.

Song, Shaojie, Hélène Angot, Noelle E. Selin, et al. (2018). „Understanding mercury oxidation and air–snow exchange on the East Antarctic Plateau: a modeling study". In: *Atmospheric Chemistry and Physics* 18.21, pp. 15825–15840.

Sprovieri, Francesca, Nicola Pirrone, Mariantonia Bencardino, et al. (2016). „Atmospheric mercury concentrations observed at ground-based monitoring sites globally distributed in the framework of the GMOS network". In: *Atmospheric Chemistry and Physics* 16.18, pp. 11915–11935.

Stamenkovic, Jelena, Seth Lyman, and Mae S. Gustin (2007). „Seasonal and diel variation of atmospheric mercury concentrations in the Reno (Nevada, USA) airshed". In: *Atmospheric Environment* 41.31, pp. 6662–6672.

Supplemental Finding That It Is Appropriate and Necessary To Regulate Hazardous Air Pollutants From Coal- and Oil-Fired Electric Utility Steam Generating Units (2015). In: *80 Fed. Reg. 75025, (to be codified at 40 C.F.R. pt. 63)*.

UN Environment Program (2019). *Global Mercury Assessment 2018*. UN Environment Programme, Chemicals and Health Branch Geneva, Switzerland.

US EPA (2018). *National Emissions Inventory (NEI)*. US EPA. URL: https://www.epa.gov/air-emissions-inventories/national-emissions-inventory-nei (visited on May 19, 2019).

– (2019). *Toxics Release Inventory (TRI) Program*. URL: https://www.epa.gov/toxics-release-inventory-tri-program (visited on May 19, 2019).

Wofsy-Munger Group on Biosphere-Atmosphere Exchange (2019). *Boston Pollutant Data.*

Zhang, L, J R Brook, and R Vet (2003). „A revised parameterization for gaseous dry deposition in air-quality models". In: *Atmos. Chem. Phys.* P. 16.

Zhang, Leiming, L. Paige Wright, and Pierrette Blanchard (2009). „A review of current knowledge concerning dry deposition of atmospheric mercury". In: *Atmospheric Environment* 43.37, pp. 5853–5864.

Zhang, Yanxu, Daniel J. Jacob, Stephanie Dutkiewicz, et al. (2015). „Biogeochemical drivers of the fate of riverine mercury discharged to the global and Arctic oceans". In: *Global Biogeochemical Cycles* 29.6, pp. 854–864.

Zhang, Yanxu, Hannah Horowitz, Jiancheng Wang, et al. (2019). „A Coupled Global Atmosphere-Ocean Model for Air-Sea Exchange of Mercury: Insights into Wet Deposition and Atmospheric Redox Chemistry". In: *Environmental Science & Technology* 53.9, pp. 5052–5061.

List of Figures

List of Tables